Computationally Efficient Approaches for Blind Adaptive Beamforming in SIMO-OFDM Systems

Bo Gao

Department of Electrical & Computer Engineering
McGill University
Montreal, Canada

May 2009

A thesis submitted to McGill University in partial fulfillment of the requirements for the degree of Master.

© 2009 Bo Gao

Abstract

In single-input multiple-output (SIMO) systems based on orthogonal frequency division multiplexing (OFDM), adaptive beamforming at the receiver side can be used to combat the effect of directional co-channel interference (CCI). Since pilot-aided beamforming suffers from consuming precious channel bandwidth, there has been much interest in blind beamforming approaches that can adapt their weights by restoring certain properties of the transmitted signals. Within this class of blind algorithms, the recursive least squares constant modulus algorithm (RLS-CMA) is of particular interest due to its good overall CCI cancelation performance and fast convergence. Nevertheless, the direct use of RSL-CMA within a SIMO-OFDM receiver induces considerable computational complexity, since a distinct copy of the RLS-CMA must be run on each individual sub-carriers. In this thesis, we present two approaches to reduce the computational complexity of SIMO-OFDM beamforming based on the RLS-CMA, namely: frequency interpolation and distributed processing. The former approach, which exploits the coherence bandwidth of the broadband wireless channels, divides the sub-carriers into several contiguous groups and applies the RLS-CMA to a selected sub-carrier in each group. The weight vectors at other frequencies are then obtained by interpolation. The distributed processing approach relies on the partitioning of the receiving array into sub-arrays and the use of a special approximation in the RLS-CMA. This allows a partial decoupling of the algorithm which can then be run on multiple processors with reduced overall complexity. This approach is well-suited to collaborative beamforming in multi-node distributed relaying. Through numerical simulation experiments of a SIMO-OFDM system, it is demonstrated that the proposed modifications to the RLS-CMA scheme can lead to substantial computational savings with minimal losses in adaptive cancelation performance.

Résumé

Dans les systèmes à une entrée et à multiples sorties (SIMO, soit single-input multiple output) basés sur le multiplexage par répartition orthogonale de la fréquence (OFDM, soit orthogonal frequency division multiplexing), la formation de faisceaux adaptatifs du côté du récepteur peut être utilisée pour combattre l'effet de brouillage directionnel à l'intérieur d'un même canal. Puisque la formation de faisceaux à l'aide de pilotes présente l'inconvénient d'utiliser la bande passante convoitée des canaux, il existe beaucoup d'intérêt pour les approches aveugles de formation de faisceaux qui peuvent adapter leurs poids en restaurant certaines propriétés des signaux transmis. Parmi cette classe d'algorithmes aveugles, l'algorithme à module constant suivant la méthode des moindres carrés récursive (RLS-CMA, soit recursive least squares constant modulus algorithm) présente un intérêt particulier de par son efficacité globale d'élimination de brouillage dans un même canal et sa convergence rapide. Néanmoins, l'utilisation directe d'un RLS-CMA dans un récepteur SIMO-OFDM crée une complexité informatique considérable, puisqu'il faut exécuter une copie distincte du RLS-CMA dans chaque sous-porteuse individuelle. Dans la présente thèse, nous présenterons deux approches pour réduire la complexité informatique de la formation de faisceaux SIMO-OFDM basée sur le RLS-CMA : l'interpolation des fréquences et le traitement réparti. La première approche, qui exploite la largeur de bande de cohérence des canaux sans fil à large bande, divise les sous-porteuses en plusieurs groupes contigus et applique le RLS-CMA à une sous-porteuse choisie dans chaque groupe. Les vecteurs de poids aux autres fréquences sont alors obtenus par interpolation. L'approche par traitement réparti est basée sur le partitionnement du réseau de réception en sous-réseaux et sur l'utilisation d'une approximation spéciale dans le RLS-CMA. Cela permet un découplage partiel de l'algorithme, qui peut alors être exécuté sur de multiples processeurs en réduisant la complexité globale. Cette approche est bien adaptée à la formation de faisceaux en collaboration dans les systèmes multi-noeuds à relais distribués. Grâce à des expériences de simulation numérique d'un système SIMO-OFDM, nous démontrons que les modifications proposées au schéma RLS-CMA peuvent mener à des économies informatiques non négligeables avec des pertes minimes dans l'élimination adaptative du brouillage.

Acknowledgments

I have been studying for two and half years in the permit of my master's degree in electrical engineering. During this period of time, I have learnt both academic knowledge and a positive living attitude. With my supervisor, parents and friends' help, I have completed my master's research, and finally have a chance to give my appreciation to all of you.

First, I would like to thank my supervisor Dr. Champagne. He was the one, who directed me to follow the right research track and avoid losing precious time. He was always supportive to give advice, and showed me the method and attitude to face new problems. I had some difficult time during my study, without his help, I could not make this far.

Secondly, I should say thank you to my parents. Same as most of the parents, their love to me is selfless. Since I am the only child in my family, they have done the most they could to create the best growing up environment only for me. I want to thank them for both their moral influence, and economic support. I would like to give this thesis report as a gift to them.

Finally, I show great appreciation to my girlfriend, Yinan Xu, and all others, who were companying me during the past two years. Your help will always be remembered.

Contents

List of Figures

List of Tables

List of Acronyms

SIMO	Single-Input Multiple-Output
MIMO	Multiple-Input Multiple-Output
OFDM	Orthogonal Frequency Division Multiplexing
CP	Cyclic Prefix
CCI	Co-Channel Interference
ISI	Inter Symbol Interference
ICI	Inter Carrier Interference
FM	Frequency Modulation
PM	Phase Modulation
BPSK	Binary Phase Shift Key
QAM	Quadrature Amplitude Modulation
ULA	Uniform Linear Array
AF	Array Factor
AV	Array Vector
AOA	Angle Of Arrival
CMA	Constant Modulus Algorithm
LMS	Least Mean Square
SD	Steepest Descent
RLS	Recursive Least Squares
LS	Least Squares
rms	root mean square
SNR	Signal to Noise Ratio
SINR	Signal to Interference and Noise Ratio
BER	Bit Error Rate

DFT	discrete Fourier Mransform
FFT	Fast Fourier Mransform
IFFT	Inverse Fast Fourier Transform
AWGN	Additive White Gaussian Noise
TX	Transmitter
RX	Receiver
MVDR	minimum-variance distortionless response

Chapter 1

Introduction

Today's increasing demand for high data rate transmissions continues to spur the search of improved signal processing techniques for wideband wireless communication systems. Consideration of fundamental issues in the design of these systems, such as the frequency selective fading due to multipath propagation and receiver complexity, naturally leads to the use of orthogonal frequency division multiplexing (OFDM) techniques.

OFDM splits the wideband channel into a number of sub-channels with smaller bandwidth, so that each sub-channel is experiencing near flat fading [1, 2, 3]. As a multi-carrier modulation technique, OFDM converts single high speed data stream into multiple low speed data streams, and modulates them onto different sub-carriers. These parallel sub-carriers are allocated as close to each other as possible without breaking the orthogonality among them. As a result, OFDM is very spectrum efficient. The frequency selective property of the dispersive radio environment is characterized by its delay spread, or coherence bandwidth, which is proportional to the inverse of the rms delay spread [4]. The smaller the coherence bandwidth, the more frequency selective the channel is. Hence, by choosing a reasonable spacing between sub-carrier corresponding to the coherence bandwidth, the original frequency selective channel can be approximated as a number of multiple and independent parallel flat channels; and by adding cyclic prefix (CP), instead of a silent guard period, inter symbol interference (ISI) is completely eliminated without losing the orthogonality of the OFDM and producing the inter carrier interference (ICI)[1], as long as the CP is larger than the delay spread [5]. Therefore, OFDM considerably simplifies the

[1]ICI is crosstalk between different sub-carriers, which means they are no longer orthogonal

implementation of the channel equalization.

In addition, to mitigate the effects of co-channel interference (CCI) originating from users at different locations, an effective approach consists of using multiple antennas at the receiver side (e.g. base-station). When the users are equipped with single-antenna terminals, as is assumed in this work, the resulting transmission channel from the desired user to the antenna array receiver defines a single-input multi-output (SIMO) system [1]. This situation is illustrated in Figure 1.1.

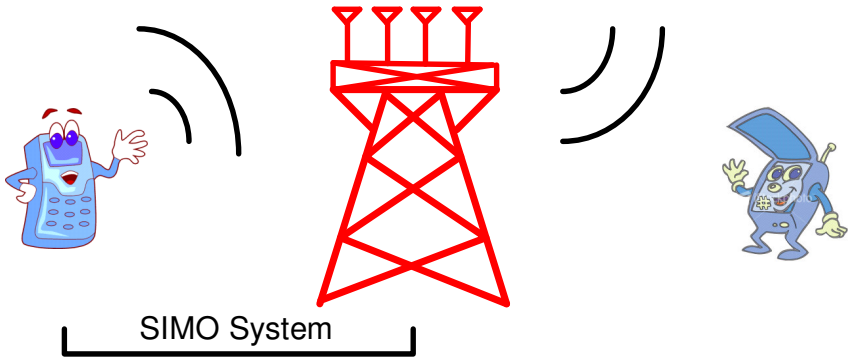

Fig. 1.1 Simple SIMO configuration for wireless communication.

In a SIMO-OFDM receiver, adaptive beamforming techniques can be applied independently on each parallel OFDM sub-channel to suppress CCI. Each beamformer iteratively computes the weights of a spatial filter so as to optimally combine the signal components originating from the desired user while rejecting signals of the same frequency but impinging upon the array from other directions. This way, the signal-to-interference-plus-noise ratio (SINR) of the desired user at the corresponding frequency can be maximized. The combination of OFDM and adaptive beamforming techniques for broadband communication has been studied in the literature. Reference [6] first studies the combination of OFDM with a pilot sequence assisted algorithm for simple matrix inversion beamforming. In [7] and [8], different blind adaptive algorithms are utilized together with the OFDM scheme. In this thesis project, a blind adaptive algorithm, recursive least squares constant modulus algorithm (RLS-CMA), will be applied to the SIMO-OFDM system, for slowly fading channels. A general literature review of the blind beamforming techniques is presented in the next section.

1.1 Literature Review on Blind Adaptive Beamforming

Adaptive beamforming techniques can be implemented by using pilot (or training) sequences to drive the iterative weight optimization process and so form adequate beampatterns [9]. However, this approach requires the allocation of precious system bandwidth which may not be available for data transmission. To overcome this limitation, there has been much interest in blind beamforming approaches that can adapt their weights by restoring certain properties of the transmitted signals.

Many communication signals have the constant modulus (CM) property, such as frequency modulation (FM), phase modulation (PM), binary phase shift key (BPSK), and Quadrature Amplitude Modulation (QAM). The amplitude of these signals is invariant with changing phase or frequency. In this respect, blind techniques based on the so-called CM criterion approach have been widely used due to their good overall CCI cancelation performance. The key goal of the CM algorithms is to recover the CM property from the received signals, which are corrupted by the propagation channel and interfering wave.

In recent years, various CM algorithms have been developed based on different optimality and search criteria. Among these, the constant modulus algorithm (CMA), which is based on least mean square (LMS) approach has attracted much interest. As demonstrated in [10], the performance of the CMA strongly depends on the selected value of step size. In [11], a least squares constant modulus algorithm (LS-CMA) is proposed based on a least square (LS) formulation of the problem; this algorithm uses a block updating scheme. Within the class of LS-based blind algorithms, the recursive least squares constant modulus algorithm (RLS-CMA) is of particular interest due to its good overall CCI cancelation performance and fast convergence. The details of RLS-CMA, which is based on the standard RLS [9], have been presented in [12, 13], and the comparison to other blind adaptive criteria were also established. Through the simulation results, [12] and [13] have verified that the RLS-CMA offers the best convergence property for both cyclostationary signals and random stationary signals respectively. In [14], more comparisons have been made among adaptive algorithms, and the RLS-CMA was also modified to a multi-modulus algorithm (MMA) to work for high order QAM constellations.

1.2 Problem Addressed and Motivation

Since OFDM allows flat fading channel techniques, such as RLS-CMA, to be applied to the broadband communication for data processing, and RLS-CMA has been proved to offer good convergence property, the SIMO-OFDM beamforming system is suitable for the urban dispersive mobile radio environment. Nevertheless, the direct use of RSL-CMA within a SIMO-OFDM receiver induces considerable computational complexity. Indeed, the RLS-CMA adaptation involves the calculation of the inverse correlation matrix of the input data, and its complexity is of order K^2, i.e. $\mathcal{O}(K^2)$[2], where K is the length of the weight vector. Also, a distinct copy of it must be run on each individual OFDM sub-carrier, for a total complexity of $\mathcal{O}(NK^2)$ per iteration, where N is the number of sub-carriers. For instance, the IEEE 802.11a OFDM model has 48 data sub-carriers [15], and accordingly, the RLS-CMA has to be applied 48 times individually to the system.

Since the complexity is the major issue of the SIMO-OFDM beamforming system, the objective of this thesis is to develop methods which can mitigate this short coming. Most of the time, complexity reduction is accompanied by a decrease in system performance as a trade off. Therefore, the goal of the thesis is to compromise between the system performance and the computational complexity.

1.3 Thesis Contribution

In this thesis, we propose two approaches to reduce the computational complexity of the SIMO-OFDM beamforming system based on the RLS-CMA, namely: frequency domain interpolation and spacial domain distributed processing.

1.3.1 Interpolation

Some interpolation-based methods to reduce the complexity of the channel estimation of the Multiple-Input Multiple-Output (MIMO) OFDM system were developed in recent years. For instance, [16] proposed a zero-forcing filter interpolation, by exploiting the fact that the adjoint and the determinant of a polynomial channel matrix is still polynomial, and

[2]In this thesis the big big order notation $\mathcal{O}(x) = \alpha(x)+\phi(x)$ notation is frequently used in computational complexity theory to describe how the size of the input data affects an algorithm's usage of computational resources (usually running time or memory), where $\alpha \in \Re^+$ is a constant and $\phi(x)$ is a function such that $\lim_{x\to\infty} \frac{\phi(x)}{x} = 0$.

[17] utilized the DFT-based interpolation to obtain a full estimation of the channel from reduced channel matrices in the frequency domain. In this thesis, we propose interpolation techniques that exploit the coherence bandwidth of the broadband wireless channels. For transmission of radio signals through highly correlated channels, the number of OFDM sub-carriers is much larger than the channel order. Therefore, several contiguous sub-carriers may end up experiencing similar fading conditions. This suggest that the RLS-CMA can be applied only to several selected tones, while the weight vectors of adjacent tones are obtained by interpolation. In the thesis, different interpolation approaches are developed and compared. Since the calculation complexities of the proposed interpolation schemes are much less than the RLS-CMA adaptation, and most of the weight vectors are obtained by interpolation, the system's complexity is decreased dramatically. Indeed if we assume that the RLS-CMA is applied once for every m sub-carriers, the total complexity of the system is reduced to $\mathcal{O}(\frac{N}{m}K^2)$ per iteration.

1.3.2 Distributed Processing

Distributed processing is also proposed to reduce the system complexity. It relies on the partitioning of the receiving array into sub-arrays and the use of a special approximation in the RLS-CMA. This allows a partial decoupling of the algorithm. Not only has the resulting algorithm an overall lower complexity, but it can also be run on multiple processors simultaneously. This approach is well-suited for collaborative beamforming in the multi-node distributed relaying, which is developed for energy constrained sensor networks. With this implementation, multiple sensors are able to collaboratively communicate with the base station, by forming a directive beam [18]. If the whole antenna array is divided into M sub-arrays, the system complexity is reduced to $\mathcal{O}(\frac{N}{M}K^2)$ per iteration with the proposed distributed approach.

The two methods above can also be combined. In this case, the system complexity is reduced due to both spatial and frequency domain processing, as $\mathcal{O}(\frac{N}{mM}K^2)$. However, this combination may have more important effect on the system performance, and different values of m and M should be tried for the best compromise.

1.4 Thesis Organization

The rest of the thesis is organized as follows. Chapter 2 reviews various adaptive beamforming techniques, and discuses their relative performance. Chapter 3 briefly reviews basic OFDM concepts, and then presents the SIMO-OFDM system model under consideration in this work. Chapter 4 develops the two proposed techniques for computational complexity reduction of blind SIMO-OFDM beamforming based on RLS-CMA. Simulation results of SIMO-OFDM transmission are shown and discussed in Chapter 5 to demonstrate the system performance after applying these complexity reduction techniques. Finally, Chapter 6 gives a summary of the thesis, and mentions possible future work.

Chapter 2

Adaptive Beamforming

2.1 Basic Concepts

A radio antenna is used to transmit or receive information signals propagating through space. Therefore it should be designed to achieve high gain in some particular directions, and at the same time, produce nulls in other directions to minimize the effect of undesirable interference. Normally, a suitably high gain can be achieved by controlling the physical size and transmission power. Alternatively, engineers may resort to the use of an antenna array, i.e., a collection of antennas located at specific positions in space. Through linear filtering of the spatial wave field impinging on the antennas, the antenna array system can also achieve high directive gain. This type of system is commonly used in recent wireless communication systems.

Through the use of an antenna array, spatial filtering, also called beamforming, is widely employed in wireless communication systems to separate the signals from different users, which may be highly correlated in time. Since the users have different locations in space, the separation can be achieved by an antenna array. The amplitudes and phases of the antenna elements are varied to optimize the quality of the useful signal in the presence of directional noise and interference. This is achieved through the application of complex weights to the demodulated outputs of the antennas and summing the resulting signals. In a sense, the operation is similar to discrete temporal filtering, but it is realized on spatial samples. Before going through the detail of adaptive algorithms, some basic concepts should be introduced first.

2.1.1 Uniform Linear Array (ULA)

Since different radio environments are characterized by different channel conditions, several different types of antenna geometries have been considered. Among these, three common types of array geometries that are encountered in applications include: the uniform linear array (ULA), the circular array, and the planar array. The names of these arrays are defined after their shapes. However, other geometries are possible. For example, in Ad Hoc sensor network [18], the antenna elements are randomly distributed in a certain area to do collaborative beamforming.

The model used in this thesis is based on a ULA, whose configuration is illustrated in Figure 2.1. In this figure, θ is the angle of arrival (AOA) of a propagating plane signal waveform. The same type of antennas are used in the array, and the antenna spacing, d, between adjacent elements in a constant parameter, i.e., elements are uniformly distributed. Typically, $d = \frac{\lambda}{2}$ is often applied for a good compromise between unwanted mutual coupling effects and control of ambiguity lobes, where λ is the wavelength of the transmitted signal [19], i.e., the inverse of the carrier frequency.

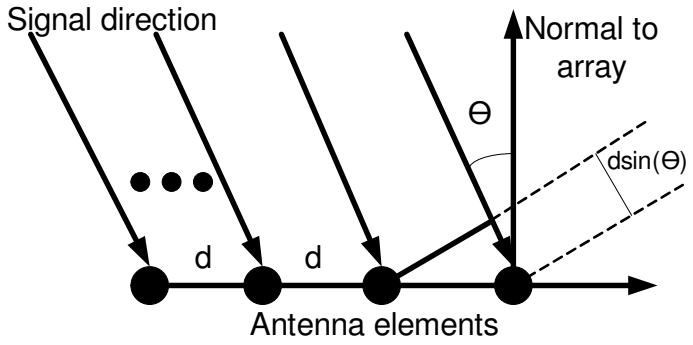

Fig. 2.1 Uniform Linear Array (ULA).

2.1.2 Fixed Beamforming

The array vector (AV), also called steering vector, is an important concept for beamforming. It characterizes the number of the elements, the geometry of the array, and the amplitude and phase of each element. When an ULA is used in the system, each element receives the same signal but with different time delays, as represented by equivalent phase shifts. Therefore, the received signal amplitude of each element is the same. Corresponding to

Figure 2.1, the AV is defined as

$$\mathbf{AV}(\theta) = [1, e^{jkdsin(\theta)}, e^{j2kdsin(\theta)}, \ldots, e^{j(K-1)kdsin(\theta)}]^T \tag{2.1}$$

where k is the steering parameter, and K is the number of the antenna elements in the array.

The weight vector of the beamforming system is designed to adjust AV in order to control the direction of the beampattern. The basic beamforming structure to compensate for the phase difference in the array vector is shown in Figure 2.2, where $[x_1(n) \cdots x_K(n)]$

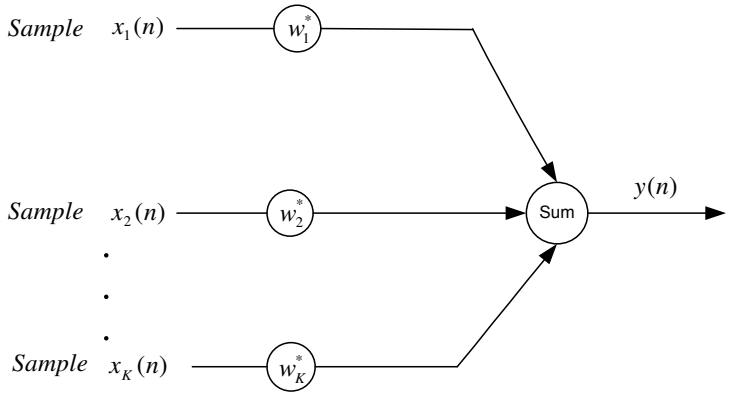

Fig. 2.2 Beamforming Structure.

denote the baseband antenna samples at discrete-time n, w_i is the complex weight applied to the i^{th} antenna output and $y(n)$ is the beamforming output, given by

$$y(n) = \sum_{i=1}^{K} w_i^* x_i(n) \tag{2.2}$$

A normalized beampattern, corresponding to weights $w_i = 1$, is shown in Figure 2.3 for a ULA with $K = 10$ antennas. In this example, the polar plot gives the response, (i.e. gain), of the beamforming system to a plane wave with AOA of $\theta \in (-90°, 90°)$. Because of the special choice of weights, the main lob is perpendicular to the ULA. If the useful signal has an AOA= 10°, by changing the amplitude and phase of the weight vector, the beampattern can be redirected to the desired direction, as shown in Figure 2.4.

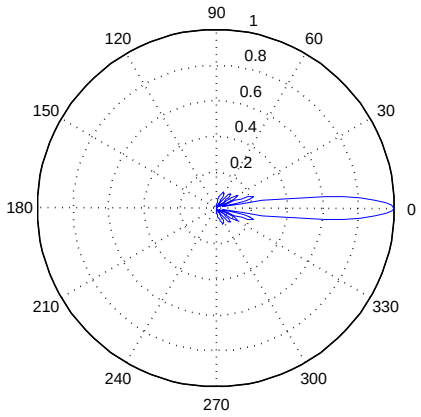

Fig. 2.3 Original beampattern (all weights set to 1).

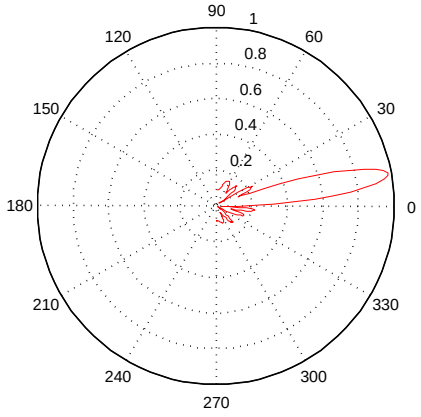

Fig. 2.4 Beampattern for steering direction of $\theta = 10°$.

2.1.3 Adaptive beamforming

Adaptive beamforming is based on similar principles, but instead of using a set of fixed antenna weights, these are updated in realtime to "best match" the changing conditions of the surrounding propagation and interference environment. This is typically achieved via feedback control aimed at restoring the quality of the output signal, $y(n)$. This can be done by exploiting the statistics of the channel, a pilot of reference signals or other structural properties. The basic adaptive beamforming structure is shown in Figure 2.5, which is modified from Figure 2.2 by adding the feedback control algorithm into the system, and allowing the weights to vary with time, i.e., $w_i(n)$.

For adaptive beamforming, several different methods or algorithms are available to ad-

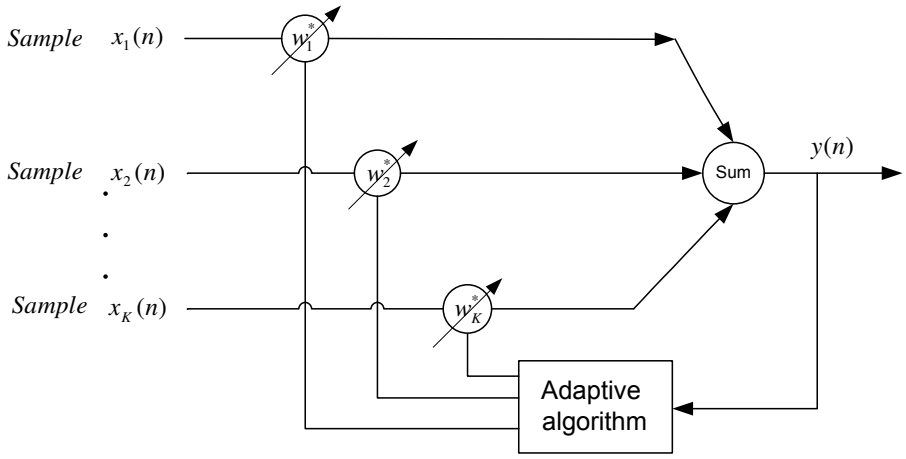

Fig. 2.5 Adaptive Beamforming Structure.

just the weights, $w_i(n)$, iteratively over time as new data $x_i(n)$ become available. The directivity of the adaptive beamforming system, represented by its beampattern, will also change with the weights, which are adjusted at each iteration. A well designed adaptive beamforming system will result in an increase of output signal quality over time, as measured by its SINR or the bit-error-rate (BER) in digital communication applications.

In general, the various adaptive beamforming algorithms can be classified into two broad categories, namely: non-blind adaptive beamforming, and blind adaptive beamforming. Both categories are discussed below.

2.2 Non-Blind Adaptive Beamforming

As mentioned above, the weight vector is utilized to adjust the beampattern to increase the quality of the signal of interest. In this section, some well-known non-blind adaptive algorithms that are available to update the weight vector are described briefly. The algorithms in this category make use of a training sequence (a pilot) to update the weight vector.

2.2.1 Least Mean Square (LMS) Algorithm

The LMS algorithm belongs to the family of stochastic gradient optimization algorithms. It is a modified form of the classic steepest descent (SD) optimization algorithm. The main difference between them is that, the LMS uses a estimated gradient rather than a deterministic gradient in the algorithm. Since the LMS is based on the SD, the latter

will be explained first. Assume $\mathbf{W}(n)$ is a $K \times 1$ weight vector at time n. The algorithm looks for the $\mathbf{W}$ which minimizes $E|\varepsilon(n)|^2$, where $\varepsilon(n) = d(n) - y(n)$. The signals are assumed stationary and E denotes expectation. The following two equations illustrate the SD approach [9],

$$\mathbf{W}(n+1) = \mathbf{W}(n) - \frac{\mu}{2}\nabla(E|\varepsilon(n)|^2) \tag{2.3}$$

$$\nabla(E|\varepsilon(n)|^2) = 2(\mathbf{R}\mathbf{W}(n) - \mathbf{p}) \tag{2.4}$$

where $\mathbf{R} = E\{\mathbf{X}(n)\mathbf{X}^H(n)\}$, and $\mathbf{p} = E\{\mathbf{X}(n)d^*(n)\}$. In these equations, $\mathbf{R}$ is the auto correlation matrix of the input vector, $\mathbf{X}(n) = [x_1(n) \dots x_K(n)]^T$, $\mathbf{p}$ is the cross correlation vector between the input vector and the desired signal (e.g. pilot), $d(n)$, and μ is the step size of the weight optimization. These two equations iteratively minimize the mean square error, $E|\varepsilon[n]|^2$, and consequently result in an optimal weight vector.

In practice, it is difficult to estimate the quantities $\mathbf{R}$ and $\mathbf{p}$. In LMS, instantaneous estimation is used instead. To implement LMS, we use vector $\mathbf{X}(n)$ to obtain instantaneous approximation to $\mathbf{R}$ and $\mathbf{p}$, i.e.

$$\mathbf{R}(n) = \mathbf{X}(n)\mathbf{X}^H(n) \tag{2.5}$$

$$\mathbf{p}(n) = \mathbf{X}(n)d^*(n) \tag{2.6}$$

Substituting (2.5) and (2.6) into (2.3), the new weight vector updating equation is obtained as:

$$\begin{aligned} \mathbf{W}(n+1) &= \mathbf{W}(n) + \mu\mathbf{X}(n)[d^*(n) - \mathbf{X}^H(n)\mathbf{W}(n)] \\ &= \mathbf{W}(n) + \mu\mathbf{X}(n)[d(n) - y(n)]^* \\ &= \mathbf{W}(n) + \mu\mathbf{X}(n)\varepsilon^*(n) \end{aligned} \tag{2.7}$$

By using this equation, the optimal weights can be obtained iteratively over time. If the iteration is sufficient long, the LMS solution may converge to the SD solution. To ensure convergence of the algorithm μ can be selected between 0 and $\frac{2}{\lambda_{max}}$, where λ_{max} is the maximum eigenvalue of $\mathbf{R}$. The step size plays a very important role in the operation of the algorithm. If its value is too small, the convergence rate of the LMS is low, and consequently, much time is consumed to obtain the optimal weight vector. Furthermore, if the signal statistics, i.e. $\mathbf{R}$ and $\mathbf{p}$, change rapidly, the algorithm with small μ is not able

to reach an optimal weight vector, due to its slow convergence. However if μ is too large, although the algorithm may converge more rapidly, the residual error will be higher than in the former case.

To illustrate these concepts, an example is shown below. Assume there is a $K = 10$ element ULA, the desired signals AOA is $10°$ and the interferers AOA is $-30°$. Both the signal and interference are assumed to have unit power, and the signal-to-noise ratio (SNR) is $10dB$. For simplicity, the AOAs are assumed to be invariant during the adaptation. In this example, $\mu = 0.01$ and $\mu = 0.005$ are selected for comparison.

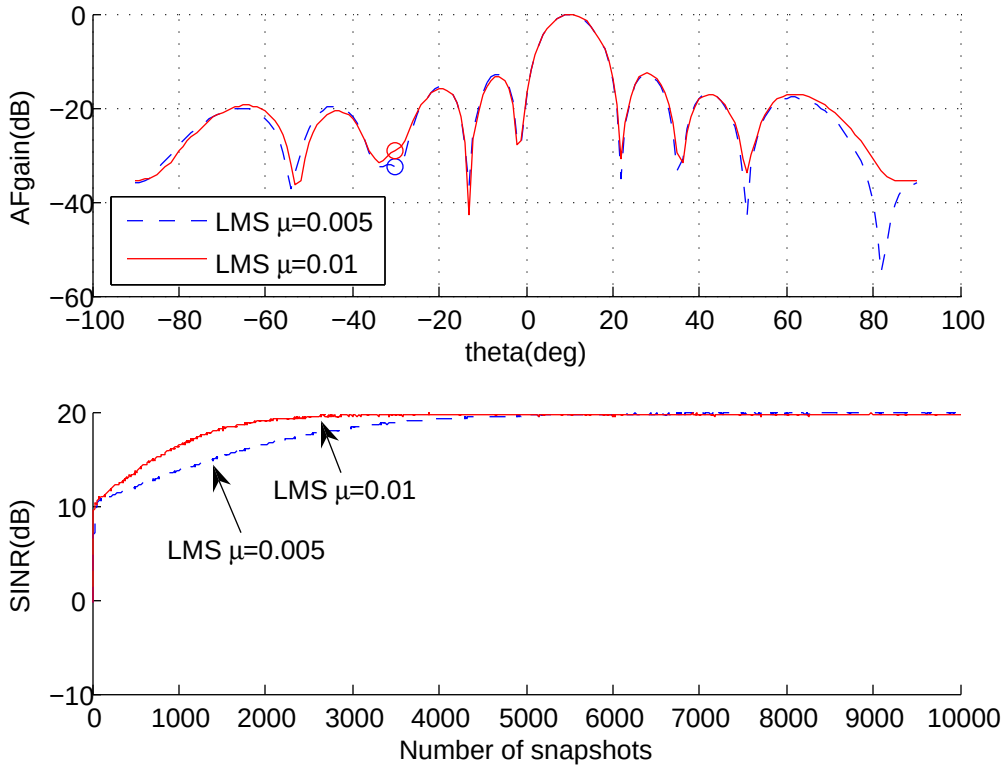

Fig. 2.6 Beampattern after convergence (top) and SINR versus iteration (bottom) for the LMS algorithm with different values of the step size μ.

As depicted in Figure 2.6, after 10^4 iterations, both beampatterns can achieve a high gain at $10°$, and a low gain at $-30°$. The one of a smaller step size $\mu = 0.005$ results in a better performance for the beampattern, i.e., a deeper null (by -5dB) in the interference direction; however, a longer time is needed for convergence. In practice, the value of μ is adjusted to achieve a proper trade-off between steady-state performance and convergence

speed.

2.2.2 Recursive Least Squares (RLS) Algorithm

The LMS algorithm has a relatively slow convergence rate, and its behavior largely depends on the step size, μ. The RLS algorithm discussed in this section offers an alternative to the LMS: its convergence rate from initialization is typically faster but its complexity is higher. The RLS is developed based on the Method of Least Square (LS). In this case, the algorithm attempts to recursively update the least square solution for the weight vector, $\mathbf{W}$, from time 0 up to current time n. A detailed algorithm derivation can be found in [9]; here, we only provide a general overview.

The cost function of the RLS is given by

$$J(n) = \sum_{i=1}^{n} \lambda^{n-i} |\varepsilon(i)|^2 = \sum_{i=1}^{n} \lambda^{n-i} |d(i) - \mathbf{W}^H \mathbf{X}(i)|^2 \tag{2.8}$$

where $0 < \lambda < 1$ is the forgetting factor, which is used to control the memory of the algorithm. The other parameters and variables are identical as those defined for the LMS algorithm. According to LS theory, the optimal weight vector that minimizes the cost function is given by

$$\hat{\mathbf{W}}(n) = \Phi^{-1}(n)\mathbf{z}(n) \tag{2.9}$$

where

$$\Phi(n) = \sum_{i=1}^{n} \lambda^{n-i} \mathbf{X}(i)\mathbf{X}^H(i) \tag{2.10}$$

$$\mathbf{z}(n) = \sum_{i=1}^{n} \lambda^{n-i} \mathbf{X}(i)d^*(i) \tag{2.11}$$

In the equations, $\Phi(n)$ is the time-average correlation matrix of the input data, and $\mathbf{z}(n)$ is the time-average cross-correlation between the input signal and the training sequence. by expressing the equations for $\Phi(n)$ and $\mathbf{z}(n)$ as 1^{st} order difference equations, and applying the matrix inversion lemma, the RLS is obtained in [9] as follows,

$$\mathbf{H}(n) = \mathbf{P}(n-1)\mathbf{X}(n) \tag{2.12}$$

$$\mathbf{G}(n) = \mathbf{H}(n)/(\lambda + \mathbf{X^H}(n)\mathbf{H}(n)) \tag{2.13}$$

$$\xi(n) = d(n) - \mathbf{W}^H(n-1)\mathbf{X}(n) \tag{2.14}$$

$$\mathbf{W}(n) = \mathbf{W}(n-1) + \mathbf{G}(n)\xi^*(n) \tag{2.15}$$

$$\mathbf{P}(n) = \lambda^{-1}\mathbf{P}(n-1) - \lambda^{-1}\mathbf{G}(n)\mathbf{X}^H(n)\mathbf{P}(n-1) \tag{2.16}$$

The initial values of the parameters are $\mathbf{W}(0) = 0$, $\mathbf{P}(0) = \delta^{-1}I_{L\times L}$, and δ is a small positive constant. In the algorithm, $\mathbf{P}(n) = \Phi^{-1}(n)$, $\mathbf{H}(n)$ is an internal parameter, and $\xi(n)$ is called a priori estimation error, which is calculated based on $\mathbf{W}(n-1)$ instead of $\mathbf{W}(n)$.

Compared to the LMS algorithm, the RLS has a faster convergence rate. However, since the algorithm includes a matrix inversion, its computational complexity is much higher. The RLS can also be applied to the example in Section 2.2.1, and the comparison results are shown in Figure 2.7. The RLS algorithm forms a better beampattern, and has a much faster convergence rate than the LMS.

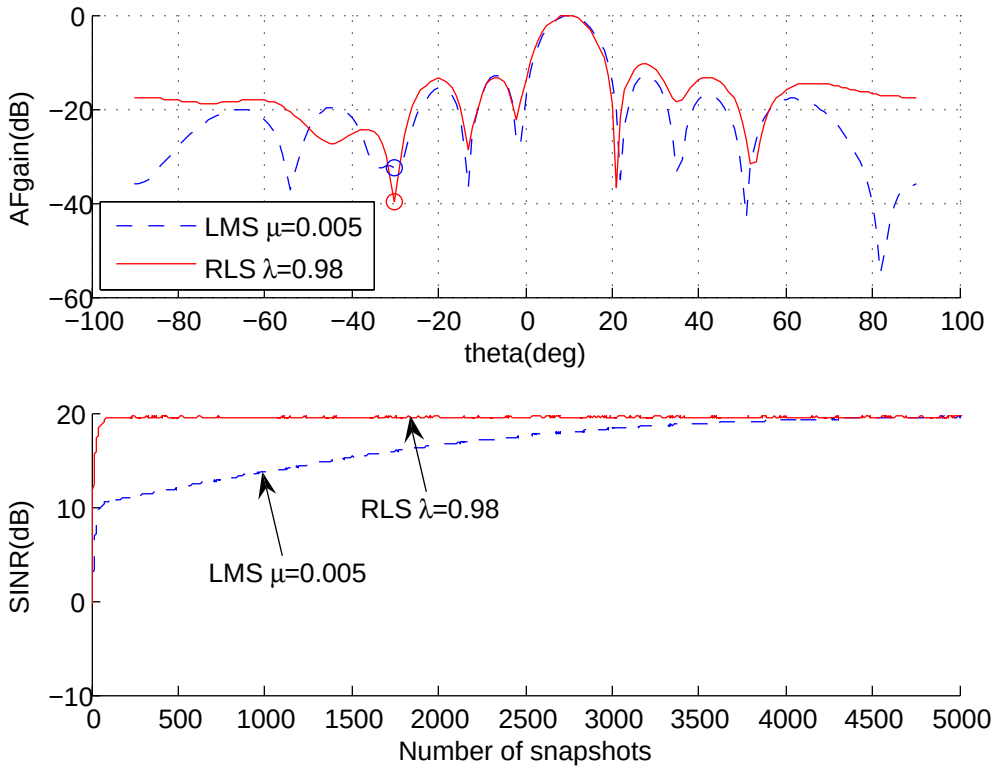

Fig. 2.7 Beampattern after convergence (top) and SINR versus iteration (bottom) for the LMS and the RLS algorithm.

2.3 Blind Adaptive Beamforming

Both of the conventional non-blind adaptive beamforming algorithms in the above section are said to be "pilot-aided", i.e. they use a training signal to update the weight. Accordingly, these methods suffer from consuming precious channel bandwidth, i.e., when the pilot is transmitted, no other useful sequences can be transmitted by the same spectrum. Sometimes it is also difficult to characterize the statistical properties of the training sequence to estimate the radio environment. To overcome these limitations, there has been much interest in blind beamforming approaches, which can adapt their weight vector by restoring certain structural properties of the transmitted signals. Many communication signals, such as FM, PM, BPSK, and some QAM signals, have the constant modulus (CM) property, which means the amplitude of the signal is constant after these modulation schemes are applied. However, this CM property is lost after the transmitted signals are corrupted by the channel effects, noise and interference. If the CM property can be restored by applying some adaptive beamforming algorithms, the source signal can be detected from the interferences, which do not have CM property, even without the help of training sequences. Algorithms, which can recover the CM property, are generally called constant modulus algorithms (CMA). Corresponding to the above discussion, both LMS and RLS based CMA will be illustrated here.

2.3.1 LMS-based CMA

As described in [10], a CMA can be developed from the LMS algorithm, by attempting to minimize the following cost function:

$$J(\mathbf{W}) = E[(|y(n)|^2 - 1)^2] \tag{2.17}$$

where $y(n)$ is the output of the antenna array beamformer. $J(\mathbf{W})$ is the mean square difference between the square of modulus of $y(n)$ and 1, which is assumed to be the CM value of the unknown source signal. The CMA looks for a weight vector such that $J(\mathbf{W})$ is minimized. The following equations are the key steps of the algorithm.

$$y(n) = \hat{\mathbf{W}}^H(n-1)\mathbf{X}(n) \tag{2.18}$$

$$\varepsilon(n) = y(n)[1 - |y(n)|^2] \tag{2.19}$$

$$\hat{\mathbf{W}}(n) = \hat{\mathbf{W}}(n-1) + \mu \mathbf{X}(n)\varepsilon^*(n) \tag{2.20}$$

In [20], this basic algorithm is further extended to variable μ, where μ is the algorithm step-size. This modification allows the algorithm to work in the fast fading channel.

Since the LMS-CMA is only considering the signal's CM property, it is phase-blind, in that the convergency of the weight vector is invariant to phase rotations in the transmitted signal constellation. Hence the received symbols may have phase offset as compared with the transmitted ones. This situation is illustrated in Figure 2.8 for a 4-QAM example. This simulation result is obtained based on passing 5000 4-QAM symbols through an additive white gaussian noise (AWGN) channel, with a co-channel interference. The "•" represents the receiver side symbol constellation with phase offset, and the "∘" represents the symbol constellation after applying a proper phase shift.

In practice, it is necessary to compensate the phase offset to obtain adequate BER performance of the system. This can be achieved by either utilizing the phase-locked loop [21], or applying a modified form of the LMS-CMA algorithm, which recovers the CM property of the signal in both real and imaginary domains separately [14, 22]. The phase-locked loop method needs additional decision-directed processing besides the LMS-CMA, while the modified CMA approach can yield a similar performance in a more efficient way. Hence, the latter method is often preferred.

2.3.2 RLS-CMA

In this section, we explain how the RLS approach can be used to develop a blind algorithm, with faster convergence rate. An approximation to the cost function in (2.17) has to be made to derive the RLS-CMA. The details of the algorithm development are described in [12, 13], while the main steps are summarized below.

First, the expectation operator in the cost function in (2.17) is replaced by an exponentially weighted time average sum as follows:

$$J(\mathbf{W}) = \sum_{k=1}^{n} \lambda^{n-k}(|\mathbf{W}^H\mathbf{X}(k)|^2 - 1)^2 = \sum_{k=1}^{n} \lambda^{n-k}(\mathbf{W}^H\mathbf{X}(k)\mathbf{X}^H(k)\mathbf{W} - 1)^2 \tag{2.21}$$

where $\lambda \in [0, 1]$ is a forgetting factor. To obtain a quadratic expression of the weight vector

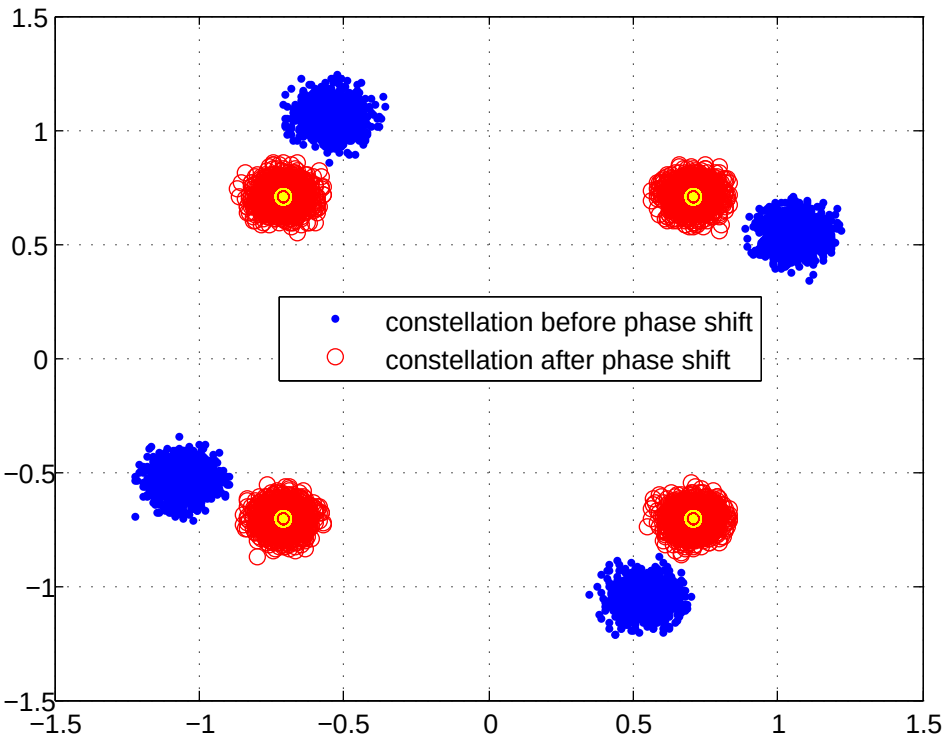

Fig. 2.8 Constellation of the received symbols before and after the phase rotation.

$\mathbf{W}$, the following approximation is made to (2.21).

$$J'(\mathbf{W}) = \sum_{k=1}^{n} \lambda^{n-k} (\mathbf{W}^H \mathbf{X}(k) \mathbf{X}^H(k) \mathbf{W}(k-1) - 1)^2 \tag{2.22}$$

In (2.22), the previously calculated weight vector, i.e. $\mathbf{W}(k-1)$ is used in place of the current weight vector, $\mathbf{W}$, to compute one of the products $\mathbf{X}^H(k)\mathbf{W}$. The resulting expression in (2.22) is now quadratic in $\mathbf{W}$. From there, the RLS-CMA is obtained by proceeding as in the derivation of the standard RLS algorithm [9]. The RLS-CMA is similar in form to the standard RLS except that it operates on the input signal vector $\mathbf{Z}(k) = \mathbf{X}(k)\mathbf{X}^H(k)\mathbf{W}(k-1)$, and the reference signal is set to a constant, 1. The RLS-CMA is summarized below.

$$\mathbf{Z}(n) = \mathbf{X}(n)\mathbf{X}^H(n)\mathbf{W}(n-1) \tag{2.23}$$

$$\mathbf{H}(n) = \mathbf{P}(n-1)\mathbf{Z}(n) \tag{2.24}$$

$$\mathbf{G}(n) = \mathbf{H}(n)/(\lambda + \mathbf{Z}^H(n)\mathbf{H}(n)) \tag{2.25}$$

$$\xi(n) = 1 - \mathbf{W}^H(n-1)\mathbf{Z}(n) \tag{2.26}$$

$$\mathbf{W}(n) = \mathbf{W}(n-1) + \mathbf{G}(n)\xi^*(n) \tag{2.27}$$

$$\mathbf{P}(n) = \lambda^{-1}\mathbf{P}(n-1) - \lambda^{-1}\mathbf{G}(n)\mathbf{Z}^H(n)\mathbf{P}(n-1) \tag{2.28}$$

where, to ensure adequate operation, the initial values of the algorithm parameters are set to $\mathbf{W}(0) = [1, 0_{1\times(K-1)}]^T$, $\mathbf{P}(0) = \delta^{-1}I_{K\times K}$ (K is the number of the antenna elements), and δ is a small positive constant (e.g. 10^{-2}).

As discussed for the LMS-CMA, a modification for phase rotation can also be applied to the RLS-CMA. In that case, (2.26) just needs to be replaced by the following steps:

$$y(n) = \mathbf{W}^H(n-1)\mathbf{X}(n) = y_r(n) + jy_i(n) \tag{2.29}$$

$$\xi(n) = [y_r(n)(\frac{1}{\sqrt{2}} - |y_r(n)|^2) + jy_i(n)(\frac{1}{\sqrt{2}} - |y_i(n)|^2)]/y(n) \tag{2.30}$$

By considering the real and imaginary parts of the signal separately, (2.29) and (2.30) can combat the constellation phase error. With this modification, the phase offset issue can be compensated. The multi-modulus algorithm (MMA) [23, 24], which works for multiple modulus modulation schemes, such as 16-QAM, 64-QAM, and even some non-square constellations schemes, can also be developed based on this phase modified CM adaptation.

At this point, it is interesting to compare the behavior of the LMS-CMA and RLS-CMA, when applied to the same simulation scenario as in Section 2.2.1, originally presented for illustrating the performance of the LMS algorithm. The simulation results, shown in Figure 2.9, indicate that the same level of performance can be obtained from the blind algorithms as their non-blind counterparts. After convergence, both blind CMA and RLS-CMA approaches will result in the formation of a high gain lobe in the direction of the desired source and deep nulls in the direction of the main interference source. As expected, the RLS-CMA has a faster convergence rate than the LMS-CMA.

Finally, it is also of interest to test the blind algorithms in a time varying radio environment, and specifically the ability of these algorithms to "re-converge" after a sudden

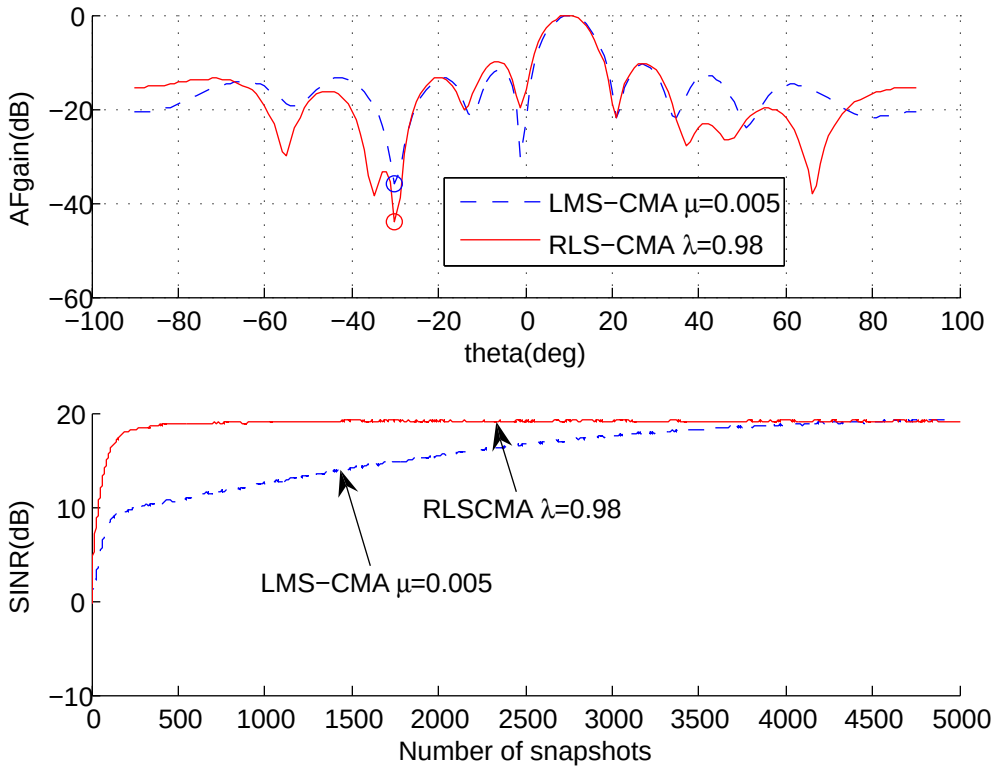

Fig. 2.9 Beampattern after convergence (top) and SINR (bottom) versus iteration for the LMS-CMA and the RLS-CMA.

change in the propagation condition. For the example presented below conditions are initially based on the previous example. At time 5000, the radio condition are changed by adding two other interference sources with different AOAs. The plot in Figure 2.10 shows that both algorithms can re-converge after the sudden change, but again, the RLS-CMA shows a better performance than the LMS-CMA.

2.4 Chapter Summary

In this chapter, a general overview of various adaptive beamforming techniques was given, and several kinds of adaptive algorithms were illustrated. These are classified into two broad categories, i.e. non-blind and blind adaptive algorithms. As illustrated with simulations, all the algorithms considered are able to obtain an optimal weight vector so as to form a high gain lobe in the desired direction, and nulls at the AOAs of interferences provided the radio channel is not experiencing very fast fading. In these examples the overall attainable

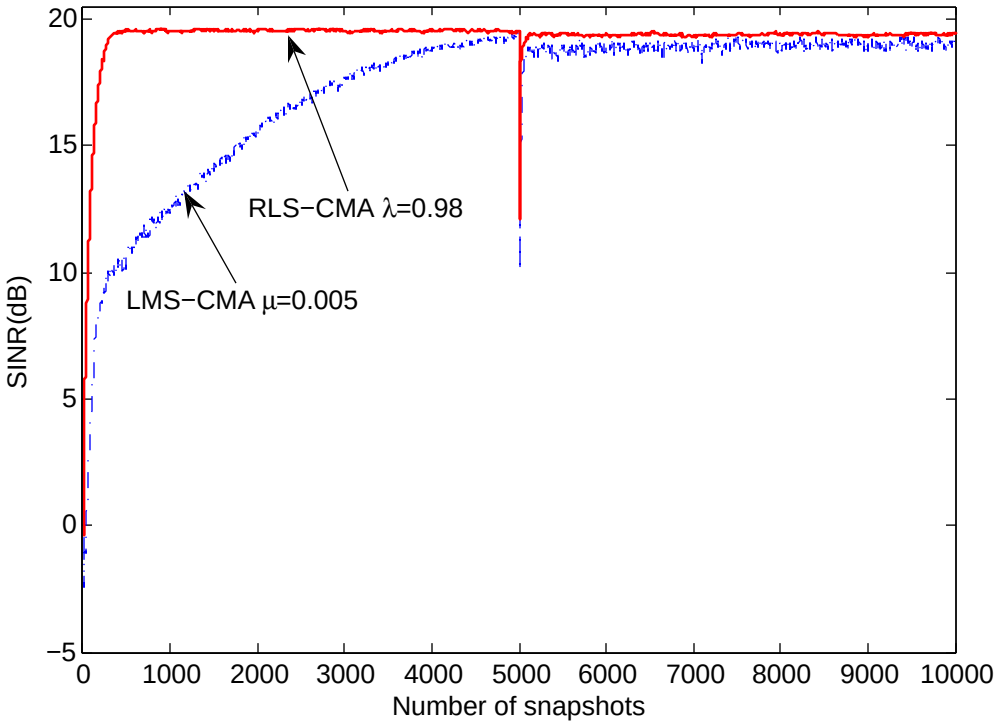

Fig. 2.10 Re-convergence ability of the LMS-CMA and the RLS-CMA.

SINR in the steady state for each algorithm is about $20dB$, when the SNR is assumed to be $10dB$. Since the non-blind algorithms need pilot sequences to carry out the adaptation process, preference is given in this work to blind approaches. While the blind LMS-CMA converges relatively slowly, the RLS-CMA is of particular interest due to its good overall co-channel interference cancelation performance and fast convergence.

Finally, we note that the adaptive beamforming (i.e. spatial filtering) algorithms discussed above were originally developed for narrow band processing scenarios. In this thesis, our interest lies in the application of these algorithms to broadband radio communications, characterized by frequency selective fading channels. To this end, we will consider these combined application with another popularly used broadband communication technique, orthogonal frequency division multiplexing (OFDM), which is further discussed in Chapter 3. The RLS-CMA is selected as the candidate algorithm for our study of blind beamforming in OFDM systems.

Chapter 3

OFDM and System Model

The increasing demand for high data rate transmission calls for broadband wireless communications. The combined requirements of frequency selective fading, due to multipath propagation, and acceptable receiver complexity for broadband communication systems naturally lead to the use of the orthogonal frequency division multiplexing (OFDM) technique. Indeed, OFDM allows the utilization of simple channel equalization techniques for data processing over the frequency selective fading channel.

In this chapter, the basic principles of OFDM are first reviewed and some of its important characteristics are given. Then, the SIMO-OFDM adaptive beamforming system, that is applied to the uplink of a broadband communication system, is presented and its performance is discussed.

3.1 OFDM

For broadband transmission systems with extremely high data rates, the transmitted signals will experience frequency selective fading, since the transmitting bandwidth is larger than the coherence bandwidth. As a result, data communication suffers from inter symbol interference (ISI), which cannot be overcome by utilizing simple channel equalization techniques. In such a situation, OFDM which is a multi-carrier transmission scheme can be applied to the system as an economical way to solve the ISI problem.

The OFDM technique is well explained in several references, including [1, 2, 3]. It is a parallel transmission scheme, which splits the single-carrier high speed transmission into multi-carrier low speed parallel transmissions. By choosing an appropriate number of sub-

carriers for transmission, the bandwidth of these parallel sub-channels is smaller than the corresponding coherence bandwidth of the entire frequency selective channel. Therefore, each sub-channel experiences flat fading, and low-cost (e.g. 1-tap) equalization technique can be applied to each of these sub-channels.

Although ISI in broadband environments can be mitigated by applying the OFDM scheme, which has been known for a long time, OFDM was not commonly used in commercial system until recently, due to its implementation complexity. However, the emergence of high-speed low-cost VLSI-based digital technologies for the calculation of the discrete Fourier transform (DFT) and its inverse (IDFT), based on the fast Fourier transform (FFT) algorithm[1], has enabled the utilization of OFDM in practical broadband wireless communications.

3.1.1 Orthogonality

The parallel sub-channels resulting from the application of the OFDM scheme overlap each other, so that, high spectral efficiency can be achieved. However, the overlapping may cause the inter channel interference (ICI) between adjacent sub-channels. One advantage of IDFT-based modulation is that the sub-carriers are appropriately shaped and spaced so as to generate correct frequency domain zero crossings. Consequently, the orthogonality between adjacent sub-channels can be preserved, and the ICI is eliminated.

By definition, two signals, $s_1(t)$ and $s_2(t)$, are orthogonal over the interval $(0, T)$ if

$$\int_0^T s_1(t)s_2^*(t)dt = 0 \tag{3.1}$$

Assume the desired OFDM system has N sub-channels equally spaced in frequency. Each sub-channel is represented by a complex exponential carrier, i.e.

$$\psi_m(t) = e^{j2\pi f_m t} \tag{3.2}$$

where f_m is the corresponding center frequency.

To ensure the orthogonality among all the sub-carriers in a multi-carrier modulation

[1]For a data vector X of size N, calculation of the FFT algorithm allows a reduction from $\mathcal{O}(N^2)$ to $\mathcal{O}(Nlog_2N)$ in the number of operations needed for the DFT of X.

system, the functions $\psi_m(t)$ should be selected such that

$$\frac{1}{T}\int_0^T \psi_m(t)\psi_i^*(t)dt = \begin{cases} 0, & m \neq i \\ 1, & m = i \end{cases} \tag{3.3}$$

where T is the OFDM symbol duration. This property can be satisfied if the individual sub-carriers are uniformly spaced in frequency with

$$f_m = \frac{m}{T} \tag{3.4}$$

Assuming, there are N such sub-carriers with index $m \in \{0, 1, \ldots, N-1\}$, the system bandwidth is then roughly given by $B = \frac{N}{T}$.

An example is given in Figure 3.1, where the orthogonality of the sub-carriers in the frequency domain is illustrated. Each of the sinc functions result from the Fourier transformation of a frequency modulated rectangular pulse. As shown in this figure, pulses modulated with carriers frequencies that differ by a multiple of $\frac{1}{T}$ do not interfere at the discrete frequency values of $\frac{m}{T}$ for $m \in \{0, 1, \ldots, N-1\}$, so that ICI is not present.

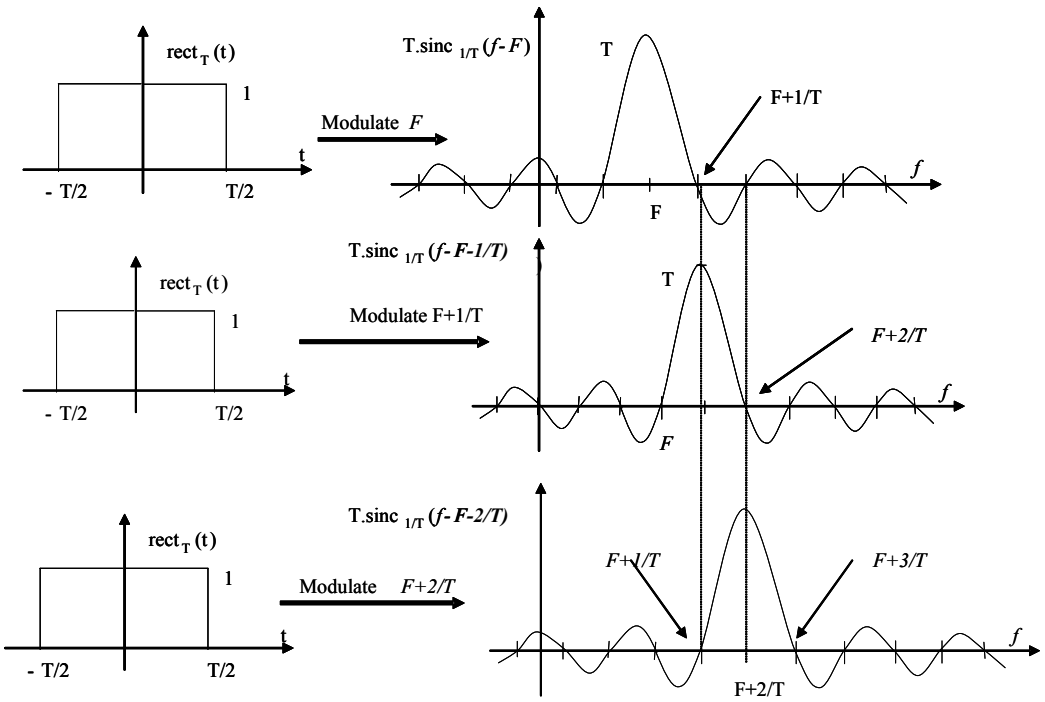

Fig. 3.1 Combining OFDM sub-carriers.

In a practical implementation of OFDM, several additional issues need to be considered, including the effect of incorrect synchronization, which relates to phase noise and frequency offset [3]. Since the perfect orthogonality of the OFDM scheme is based on both the transmitter and receiver using exactly the same frequency for each corresponding sub-carriers, both phase noise and frequency offset, due to incorrect synchronization, break the orthogonality of the sub-carriers, and consequently, result in ICI. In this thesis, the focus is on the study of an adaptive blind beamforming algorithm for the SIMO-OFDM system, and for simplicity, we shall assume that these imperfections can be neglected, i.e. incorrect propagation synchronization, which affects the orthogonality between the OFDM sub-carriers, will not be considered in the system.

3.1.2 Baseband OFDM Configuration

To simplify the presentation and without lost in generality, a baseband model is used to describe the OFDM scheme, in which shifting of the signal to the high frequency band in the transmitter (TX) and corresponding demodulation in the receiver (RX) is omitted. This system is assumed to use N orthogonal sub-carriers, and the model is built with a single transmit antenna and a single receive antenna, as depicted in Figure 3.2.

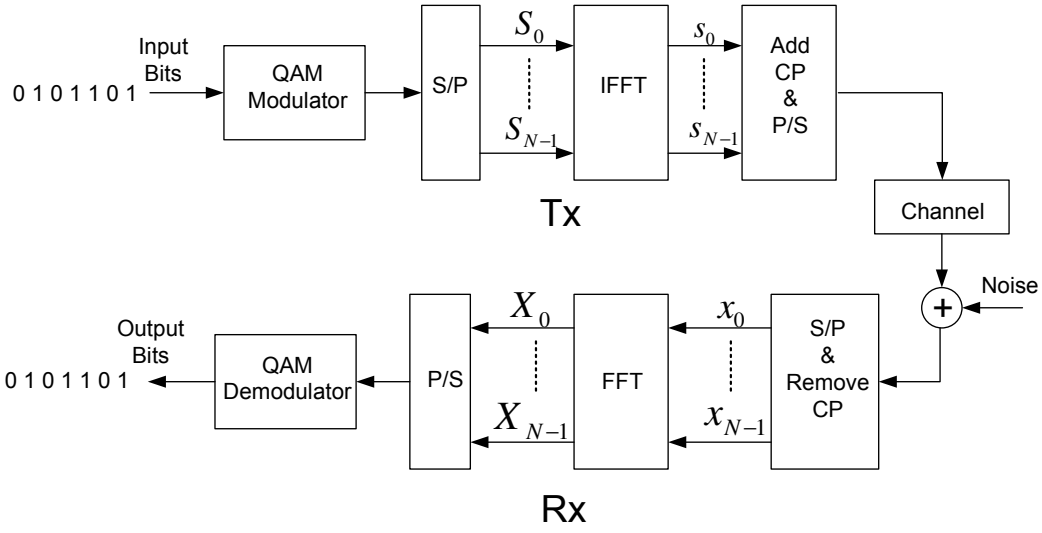

Fig. 3.2 Baseband OFDM model.

Input bits first go through a QAM-based modulator, in which they are mapped into

a sequence of complex symbols. Then by using a serial-to-parallel (S/P) converter, the modulated symbol stream is split into N sub-streams, $[S_0, S_1, \ldots, S_{N-1}]$, corresponding to the N sub-carriers. After the S/P conversion, the parallel symbol streams go through an OFDM modulator, in which the IFFT is applied as follows:

$$s_n = \sqrt{\frac{1}{N}} \sum_{k=0}^{N-1} S_k e^{j2\pi nk/N}, \quad 0 \leq n \leq N-1 \tag{3.5}$$

where k and n are the discrete frequency index and time index respectively. The IFFT operation converts the frequency symbols $[S_0, S_1, \ldots, S_{N-1}]$ into a vector of time domain samples, $[s_0, s_1, \ldots, s_{N-1}]$. Following these operations, a guard interval (GI) is added at the leading edge of each time domain vectors, which extends the length of the OFDM symbol. Finally, the OFDM symbols are converted from the parallel to serial form (P/S) for transmission over the radio channel. After going through the channel, the transmitted signal is corrupted by linear channel effects, interference, and noise. At the RX side, the baseband signal is passed through a S/P converter, and the GI is removed, resulting in a time-domain data vector $[x_0, \ldots, x_{N-1}]$. Following this step, OFDM demodulation is performed by applying the FFT, resulting in the corrupted QAM symbols, i.e. $[X_0, X_1, \ldots, X_{N-1}]$, that is

$$X_k = \sum_{n=0}^{N-1} x_n e^{j2\pi nk/N}, \quad 0 \leq k \leq N-1 \tag{3.6}$$

Finally, a QAM demodulator (or detector) is used to recover the original transmitted bits.

3.1.3 Cyclic Prefix (CP)

As mentioned previously, the use of a GI is needed in OFDM modulation. Indeed by adding and later removing the GI, wideband ISI can be mitigated, which is one of the main motivation for using OFDM as an efficient mean to deal with dispersive channels. The simplest way to create a GI, also called the silent GI, is to add a number of zeros, at the beginning of each time-domain data vector.

As shown in Figure 3.3, if the GI is longer than the expected maximum delay of the dispersive channel, the ISI can be eliminated, since the OFDM symbols, which carry the useful messages, are prevented from overlapping with each other. The GI, which does not contain directly useful information, is simply discarded at the RX. However, by adding a

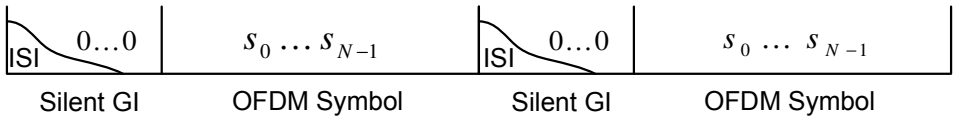

Fig. 3.3 ISI elimination by adding silent GI to OFDM time domain symbols.

silent GI, it can be shown that the orthogonality among sub-carriers is lost [3]. As described in [3, 5], it is preferable to use a CP, which is generated by repeating the last L samples of each time domain vector at their beginning, as shown in Figure 3.4.

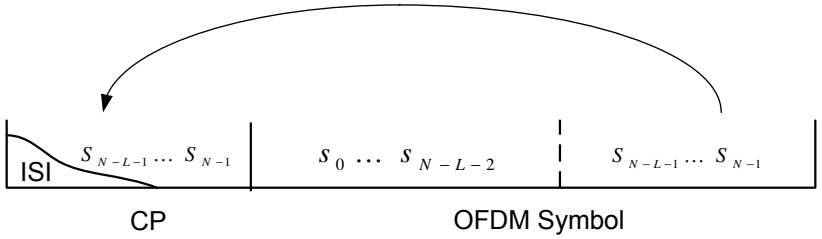

Fig. 3.4 Cyclic Prefix.

In the CP approach, instead of using a silent GT, the samples $[s_{N-L-1}, \dots, s_{N-1}]$ are inserted in front of $[s_0, s_1, \dots, s_{N-1}]$, which results in

$$\tilde{\mathbf{s}} = [s_{N-L-1}, \dots, s_{N-1}, s_0, s_1, \dots, s_{N-1}] \tag{3.7}$$

being transmitted through the channel.

Assume that for the dispersive radio environment, the channel impulse response is $[h_0, \dots, h_L]$. The channel output is the discrete time linear convolution of the input OFDM symbol stream, $\tilde{s}_n$, and the channel impulse response, h_n, plus the noise, v_n:

$$x_n \;=\; \sum_{k=0}^{L} h_k \tilde{s}_{n-k} + v_n \tag{3.8}$$

Since $\tilde{s}_n = s_{(n)_N}$ for $-L \leq n \leq N-1$, where $(n)_N$ is used in this thesis to denote n modulo N, the linear convolution (3.8) in effect corresponds to a circular convolution,

shown as follows:

$$x_n = \sum_{k=0}^{L} h_k s_{(n-k)_N} + v_n, \quad n = 0, \ldots, N-1 \tag{3.9}$$

This ensures that the sub-carriers of the OFDM scheme always differ by a multiple of $\frac{1}{T}$, which prevents the sub-channels from losing their orthogonality. Consequently, by adding the CP, multipath signals with time delay intervals smaller than the CP will not cause ICI. We note that circular convolution in time leads to multiplication in frequency. Therefore if the channel impulse response is known at the receiver, and in the absence of noise, the input symbols can be recovered by taking the FFT of the channel output:

$$S_k = \frac{X_k}{H_k} \tag{3.10}$$

where $X_k = FFT\{x_n\}$ and $H_k = FFT\{h_n\}$. Thus, besides eliminating ISI and ICI, the use of the CP facilitates the channel equalization.

Nevertheless, the OFDM scheme also has its drawbacks. One of its main disadvantages is related to the use of the CP. Indeed, since the CP is removed at the receiver side, the information contained in the CP is not utilized. Hence, the elimination of ISI comes at the cost of a reduction of the effective transmission rate, i.e. system capacity, which is due to adding the redundant CP message.

3.2 SIMO-OFDM System Model

3.2.1 System Configuration

The use of adaptive beamforming techniques in an OFDM broadband system to mitigate co-channel interference (CCI) has attracted much interest for wireless communications. Besides [6, 7, 8], as mentioned in the first chapter, some other solutions were also proposed in [25, 26] from different perspectives. The system that we are proposing in this thesis is designed for a slowly fading frequency selective radio environment. Because of the multiple antennas at the receiver side, a spatial filtering scheme can be applied to each OFDM sub-channel. Specifically, the RLS-CMA is incorporated into the SIMO-OFDM system for a broadband communication environment. One of the main advantage of the RLS-CMA is

its ability to achieve faster convergence rate.

The configuration of the system under consideration in this thesis is shown in Figure 3.5. The structure of the TX side of the system is the same as the baseband OFDM model described in Section 2, and the entire transmission bandwidth is split into N sub-carriers by applying the OFDM scheme. At the RX side, the system is equipped with K antennas. The use of the OFDM scheme enables the application of the RLS-CMA, which is capable to suppress CCI and noise received by multi-antennas, on each sub-carrier. The RLS-CMA is applied in the frequency domain after OFDM demodulation, which is called post-FFT [27]. After applying the RLS-CMA to each individual sub-carrier, the resulting signal for the k^{th} sub-carrier at the n^{th} iteration[2] is expressed as follows:

$$\hat{S}_k(n) = \mathbf{W}_k^H(n)\mathbf{X}_k(n) \tag{3.11}$$

where

$$\mathbf{W}_k(n) = [W_k^1(n), W_k^2(n), \ldots, W_k^K(n)]^T \tag{3.12}$$

$$\mathbf{X}_k(n) = [X_k^1(n), X_k^2(n), \ldots, X_k^K(n)]^T \tag{3.13}$$

After obtaining $[\hat{S}_1(n), \hat{S}_2(n), \ldots, \hat{S}_N(n)]^T$ adaptively from different sub-carriers, these symbols are P/S converted, and a QAM demodulator is used to estimate the original transmitted bits from the desired source.

We note that since the OFDM symbol duration is much longer than a single carrier system, the information updating for each sub-carrier is relatively slow. Hence, this system model is not suitable for an environment with very fast variations. In this work we assume that the coherence time of the system is much larger than the symbol period, i.e. the radio environment is experiencing slow fading, and each sub-channel is relatively unchanged during the RLS-CMA adaptation, which allows $\mathbf{W}_k(n)$ to be updated and to converge to an optimal solution for the corresponding propagation channel.

3.2.2 System Performance

As described above, by combining a SIMO-OFDM structure and adaptive beamforming, the proposed system can be used over frequency selective fading channels. A simplified example

[2]Iteration in computing is the repetition of a process within an adaptive program, such as the proposed RLS-CMA.

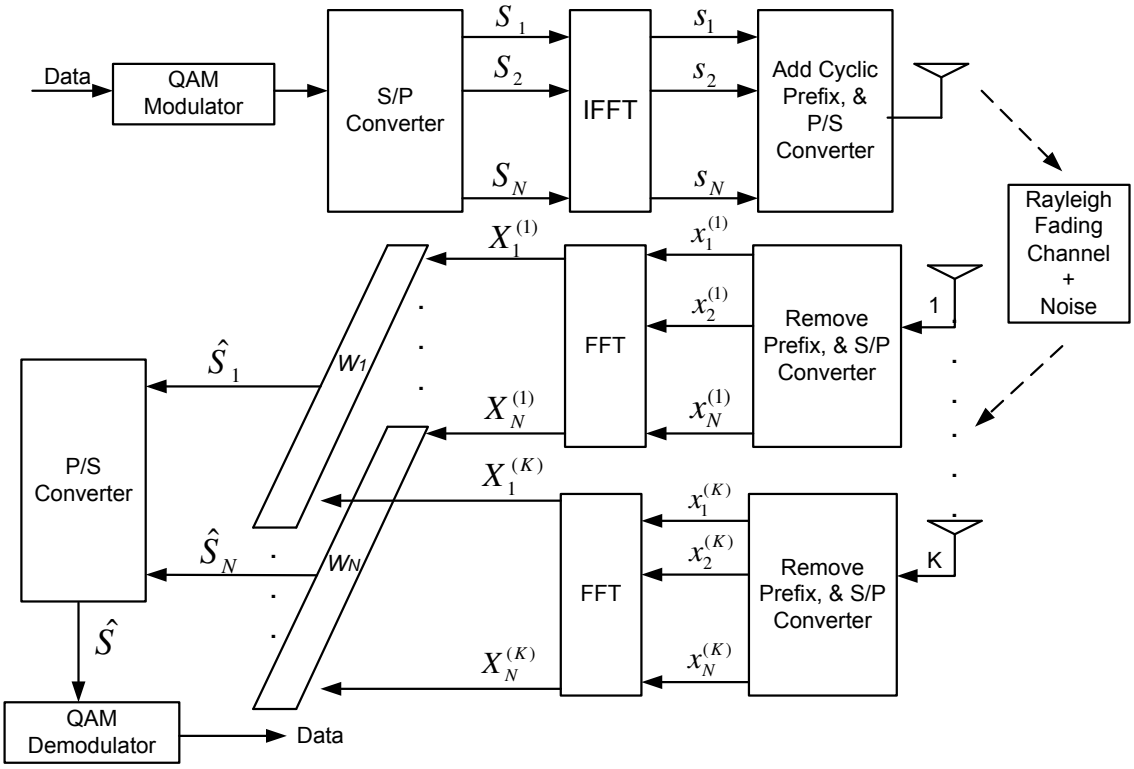

Fig. 3.5 Baseband SIMO-OFDM model.

is considered in this chapter to illustrate the operation of the system. If the K receiving antennas are closely spaced, the corresponding radio channels will be strongly correlated to each other. Therefore, for illustrative purpose, let us assume that these channels are fully correlated, i.e. all the antenna elements experience the same level of fading. The channel from the TX antenna to the j^{th} RX antenna is assumed to consist of three discrete paths with different delays, i.e.

$$h_j(k) = \mathbf{V}_j(\theta) \sum_{i=0}^{2} h_i \delta(k - iT) \tag{3.14}$$

where $\mathbf{V}_j(\theta)$ is the array vector of the j^{th} path, which contains the phase information of the antenna elements in the ULA, k is a discrete time index, T is the baseband QAM symbol duration (or the sampling period), and h_i is the amplitude of the i^{th} path. The latter is normally distributed with zero-mean and unit variance, and is taken to be the same for each antenna. The magnitude response of a signal realization of this frequency selective fading channel is shown in Figure 3.6. In this example, the 3 paths are assumed

to have the same AOA, which is $\theta = 10^o$. The OFDM scheme splits the broadband into 64 sub-channels, and the length of the CP is 8 symbols in duration, which is larger than the maximum delay of the channel to eliminate ISI. Interference is also inserted in each OFDM sub-carrier with an AOA equal to -30^o. The interference and signal power are set to the same level. At last the AWGN is added with SNR $= 10dB$.

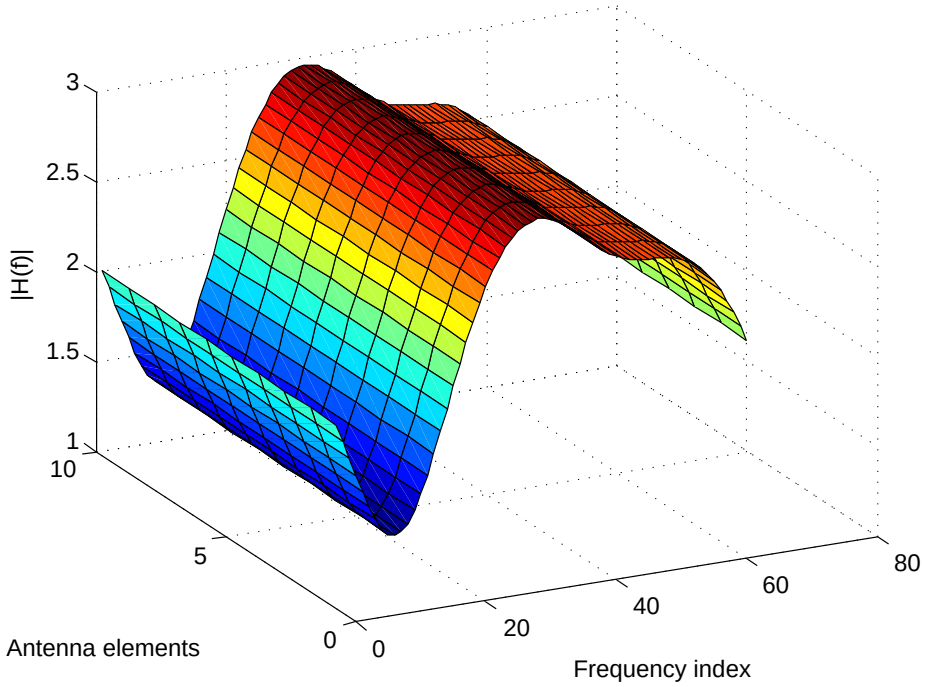

Fig. 3.6 Simplified frequency selective channel.

After applying the RLS-CMA on each sub-carrier, the beampatterns obtained after convergence are illustrated in Figure 3.7. As shown in the figure, the use of the RLS-CMA results in high gain lobes in the direction of the desired source on most of the sub-carriers, and deep nulls in the direction of the interference. However, the specific values of the beampatterns for different sub-channels are not identical. This difference depends on the characteristics of the frequency selective channel. If a certain sub-carrier is experiencing extremely deep fades, the adaptive algorithm cannot form the correct beampattern to find the desired AOA. This may eventually cause the presence of error bursts, i.e., contiguous sequences of erroneous symbols. This kind of error can be mitigated by applying pre-coding schemes, such as convolutional code and interleaving or the Reed-Solomon code [28]. For different radio environments, different coding schemes should be applied to improve the

system performance.

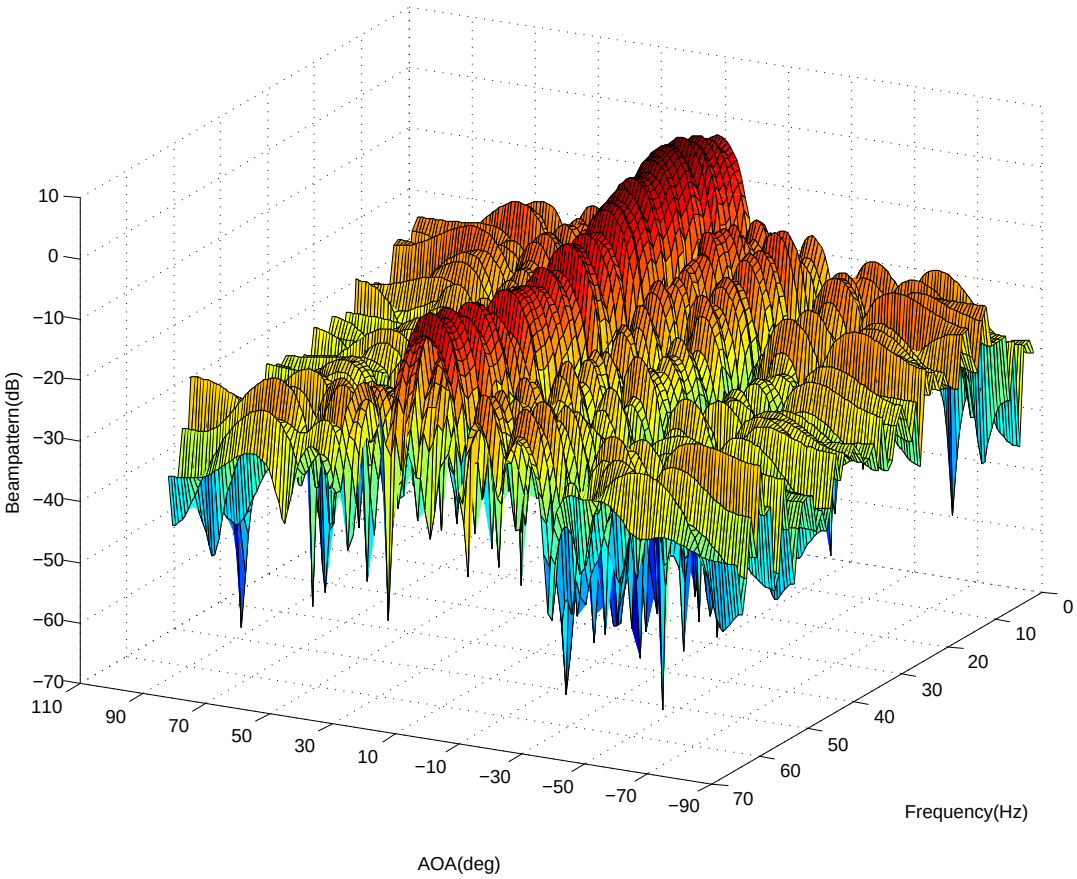

Fig. 3.7 Beampatterns obtained with the RLS-CMA in SIMO-OFDM system for all sub-carriers.

3.3 Chapter Summary

In this chapter, the OFDM multi-carrier parallel transmission technique, was briefly reviewed. It is one of the promising techniques to deal with the broadband frequency selective fading channel. It mitigates ISI by adding a cyclic prefix (CP) at the beginning of each transmitted time domain symbol. Since the sub-carriers are orthogonal to each other, the overlapping of the sub-channels, needed for spectrum efficiency, does not cause any ICI. However, since adding a CP increases the OFDM symbol duration, the elimination of ICI and ISI comes at the cost of a reduction in system capacity.

After this general presentation of the OFDM technique, the proposed SIMO-OFDM beamforming system was described, which allows the adaptive beamforming techniques to work in frequency selective fading environments for broadband wireless communication. In this thesis, the focus is on the use of RLS-CMA within the SIMO-OFDM system structure. Also, consideration is limited to slowly fading frequency selective radio environment, in which the RLS-CMA can efficiently converge to a near optimal solution and track changes in the radio channel. The corresponding system performance was also discussed.

The above simulation results indicate the capability of the proposed system to combat frequency selective fading and achieve high-gain lobes in the direction of arrival of the desired signal. However, the direct use of the RSL-CMA within a SIMO-OFDM system induces considerable computational complexity. Indeed, the RLS-CMA adaptation involves the calculation of the inverse correlation matrix of the input symbols, which has complexity of $\mathcal{O}(K^2)$ [13], where K is the length of the weight vector. Furthermore, a distinct copy of the RLS-CMA must be run on each individual OFDM sub-carrier, for a total complexity of $\mathcal{O}(NK^2)$ per iteration, where N is the number of sub-carriers. It is therefore of interest to develop and study new methods for the implementation of the RLS-CMA in SIMO-OFDM system so as to reduce the system complexity while minimizing possible losses in system performance.

Chapter 4

Reduction of System Complexity

As mentioned in the previous chapter, the direct use of the RSL-CMA within a SIMO-OFDM system induces considerable computational complexity, which is defined as the number of mathematical operations, such as summation or multiplication, involved in the system implementation. In this chapter, we propose to reduce the system complexity by exploiting both the frequency domain and the space domain. In the frequency domain, similar to [16, 17], an interpolation scheme is utilized. In this case, an adaptive algorithm is applied only to selected tones, while the weight vectors of the other tones are obtained by interpolation. In the space domain, the processing complexity can be reduced by partitioning the receiving array into sub-arrays and using a special approximation in the RLS-CMA. This allows a partial decoupling of the algorithm which can then be run on multiple processors with reduced overall complexity. Both of these methods for system complexity reduction are developed in detail as follows.

4.1 Interpolation

In the frequency domain, when applying the OFDM scheme over a channel with a relatively large coherence bandwidth, it is possible that a number of adjacent sub-carriers experience similar fading conditions. This will be the case if the number of OFDM sub-carriers is much larger than the order of the channel impulse response, as illustrated in Figure 4.1. In such a situation, it is reasonable to assume that an optimal weight vector generated for a selected sub-carrier may remain valid for neighboring sub-carriers. As a practical example, if IEEE 802.11a OFDM standard scheme is applied to a frequency selective channel with

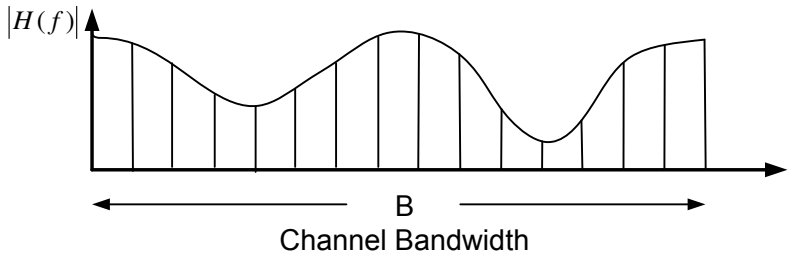

Fig. 4.1 Coherence bandwith versus OFDM sub-carriers.

a coherence bandwidth of 1.25MHz, groups of 4 sub-carriers will experience similar fading, since the subcarrier spacing for IEEE 802.11a is 312.5kHz [15].

These considerations suggest that we may divide all the sub-carriers into several groups, as shown in Figure 4.2, and apply the RLS-CMA to a selected sub-carrier in each group to calculate the optimal weight vector corresponding to it. The optimal weight vectors for the other tones in the group will be obtained by applying an interpolation scheme, such as those available to reconstruct a function from a set of corresponding sample values.

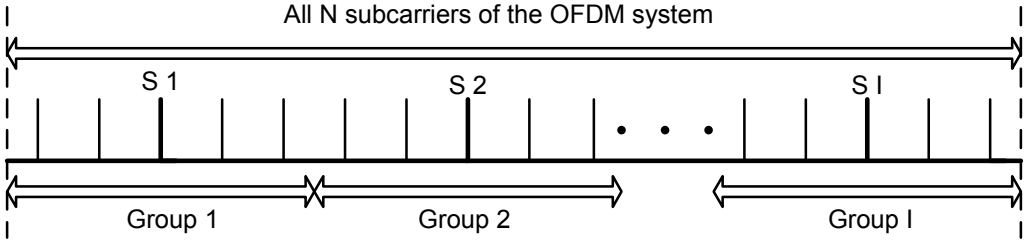

Fig. 4.2 Select OFDM sub-carriers into groups.

Before going through each interpolation scheme in detail, some corresponding indices will be defined for the system. Assume there are N sub-carriers in the OFDM system, and the interpolation group size is M. Hence, the system is divided into I groups, where $N = IM$. In general, the m^{th} sub-carrier in the i^{th} group can be defined as $\omega_m^i = \frac{2\pi(Mi+m)}{N}$, where $m \in \{0, \ldots, M-1\}$, and $i \in \{0, \ldots, I-1\}$. These indices will be used for all interpolation methods being discussed below.

4.1.1 DFT-based Interpolation

The DFT-based interpolation, used in [17] for channel estimation, could be adopted to interpolate the weight vectors. In this approach, the weight vector at the frequency $\omega_k =$

$\frac{2\pi k}{N}$, for $k \in \{0, \ldots, N-1\}$ is obtained as

$$\begin{aligned} \mathbf{W}(\omega_k) &= \mathrm{DFT_N}(\mathrm{IDFT_I}(\mathbf{W}(\omega_0^i)) + (\mathrm{ZeroPad})) \\ &= \sum_{n=0}^{N-1} \{\frac{1}{I} \sum_{i=0}^{I-1} \mathbf{W}(\omega_0^i) e^{j\omega_0^i n}\} e^{-j\omega_k n} \end{aligned} \tag{4.1}$$

where ω_0^i indicates the first sub-carrier in the i^{th} group, and the weight vector for this sub-carrier is estimated by applying the RLS-CMA.

In practice, the DFT can be implemented via FFT to reduce the complexity. Yet, the computational cost of the interpolation (4.1) is still high, as will be shown in the next section. In this thesis, two other interpolation schemes, i.e. zero order (flat-top) interpolation and first order (linear) interpolation, are chosen to avoid the increase in system complexity associated with the use of the DFT. Indeed, both of them are simpler to implement and require many less operations than the DFT-based interpolation.

4.1.2 Flat-top Interpolation

Flat-top interpolation, also called zero-order hold [29], is the simplest interpolation scheme. By definition, it maintains the level of the function to be interpolated constant between known sample values (see Figure 4.3).

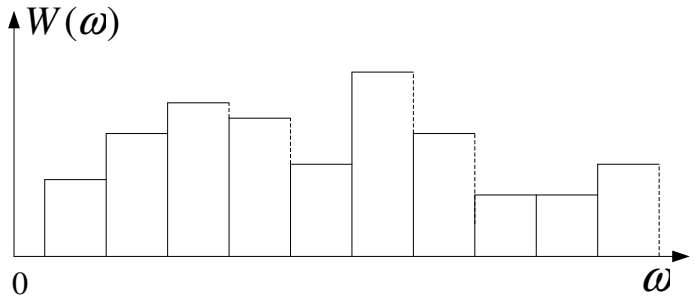

Fig. 4.3 Flat-top interpolation.

To implement flat-top interpolation for our wireless communication system, we first divide the OFDM sub-carriers into several groups with equal size. We then apply the RLS-CMA to a selected sub-carrier in each group, and the remaining members in a group use the same weight vector as the one obtained for the selected sub-carrier.

Since our system employs blind beamforming to save the spectrum, there is no side information available to guide us in the selection of a representative sub-carrier. For instance, it is possible that the tone selected to calculate the weight vector is in deep fade. Another issue that needs to be considered is the selection of the proper group size. If the group size is much greater than the coherence bandwidth, the sub-carriers in one group may experience highly different channel fades, and the weight vector obtained from the selected sub-carrier by applying RLS-CMA may not be suitable for the other group members. In this work, the sub-carrier located in the middle of the group is selected for the adaptation. This minimizes the spectral distance between the representative sub-carrier and the interpolated frequency, which helps maintaining an adequate correlation between these two frequencies. Different group sizes are also tried; in practice, the size which offers the best compromise between the computation complexity and the system performance should be chosen.

The details of the flat-top interpolation approach can be formulated as follows. Let $r_i = iM + \frac{M}{2}$ for $i \in \{0 \dots I-1\}$ denote the index of the middle tone in each group. We apply the RLS-CMA to estimate the optimal weight vector, $\mathbf{W}_{r_i}(n)$, for each of the selected tones, r_i, i.e.:

$$\mathbf{W}_{r_i}(n) = \text{RLS-CMA}(\mathbf{W}_{r_i}(n-1), \mathbf{X}_{r_i}(n)) \tag{4.2}$$

where $\mathbf{X}_{r_i}(n)$ is the input vector for the representative tone. All the remaining tones in a group use this adaptive weight vector, that is

$$\mathbf{W}_{iM+m}(n) = \mathbf{W}_{r_i}(n) \tag{4.3}$$

where $m \in \{0 \dots M-1\}$ and $m \neq \frac{M}{2}$.

4.1.3 Linear Interpolation

If the radio propagation channel is more frequency selective, i.e. the group members are not experiencing similar fades, flat-top interpolation may not be sufficient to achieve a good system performance. In this case, linear interpolation can be used instead to improve the system performance without adding much complexity. The linear interpolation scheme, whereby adjacent selected samples are connected by a straight line [29], is illustrated in Figure 4.4. In this case, instead of using the same weight vector for all the group members,

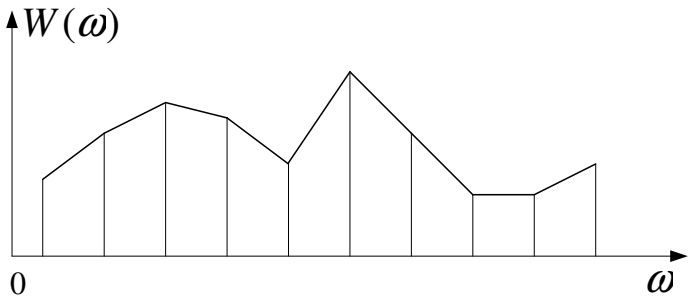

Fig. 4.4 Linear interpolation.

the weight vectors of the sub-carriers between two selected tones are obtained by applying linear interpolation between $\mathbf{W}_{r_i}(n)$ and $\mathbf{W}_{r_{i+1}}(n)$. The direct application of a linear interpolation scheme would lead to the following equation,

$$\mathbf{W}_l(n) = \frac{r_{i+1} - l}{M}\mathbf{W}_{r_i}(n) + \frac{l - r_i}{M}\mathbf{W}_{r_{i+1}}(n) \tag{4.4}$$

where $l \in \{r_i \dots r_{i+1}\}$ and $i \in \{0 \dots I-2\}$.

Perhaps surprisingly, equation (4.4) fails to perform properly. A simple example is considered to explain this problem. Assume there is only a single antenna at the RX side. Hence, instead of a weight vector, each sub-carrier is characterized by a single complex weight. The problem is that each copy of the blind RLS-CMA will introduce an ambiguous phase factor in the estimation of $W_{r_i}(n)$. The presence of these phase factors render the direct application of linear interpolation impractical. Indeed, from Figure 4.5, vector $\vec{OA}$ represents the interpolated weight between W_{r_i} and $W_{r_{i+1}}$ in the complex plane. From the figure, we note that $|\vec{OA}| \neq \frac{R_i+R_{i+1}}{2}$ and in general, the interpolated weight fails to provide a meaningful solution for the corresponding tone. Therefore, the linear interpolation scheme needs to be modified to properly handle phase ambiguity.

To see how this can be done, the characteristic of the RLS-CMA needs to be reviewed. As a member of the CM family of algorithms, the RLS-CMA updates its weight vector based only on the modulus of the incoming symbols, i.e., it is phase-blind. Therefore, the weight vector convergency is invariant to a phase rotation, and the weight vector can achieve the optimal operation point with arbitrary phase shift, as long as the correlation between adjacent elements in the vector is kept the same. For instance, if $\mathbf{W}_l(n)$ is optimal for the tone l, $\mathbf{W}_l(n)e^{j\phi}$ is also an optimal weight vector for this tone, where $\phi \in (-\pi, \pi]$. Hence,

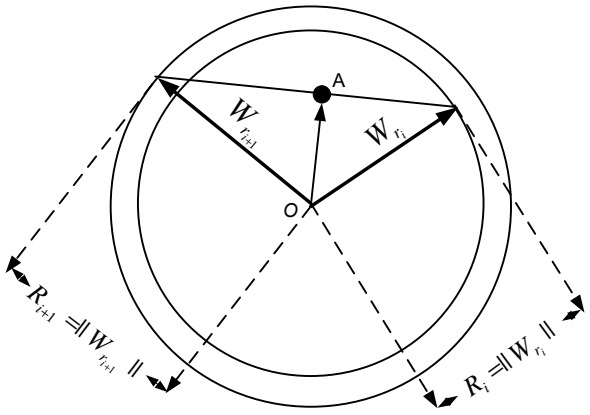

Fig. 4.5 Linear interpolation with phase error in the complex plane.

because of this phase ambiguity, the weight vectors obtained by directly applying linear interpolation to $\mathbf{W}_{r_i}(n)$ and $\mathbf{W}_{r_{i+1}}(n)$, may not work for an intermediate tone. To solve this phase ambiguity problem, we propose that before implementing linear interpolation, the weight vectors obtained by the RLS-CMA should be rotated to minimize the phase difference between them. Specifically, we propose a least-square approach in which the required phase shift is obtained by minimizing the following equation:

$$||\mathbf{W}_{r_i}(n) - e^{j\phi}\mathbf{W}_{r_{i+1}}(n)||^2 \tag{4.5}$$

in which ϕ is the phase difference between the weight vectors of the adjacent selected tones. Using standard optimization techniques, the solution to this problem is obtained as:

$$\begin{aligned} \phi_0 &= \arg\min_{\phi} ||\mathbf{W}_{r_i}(n) - e^{j\phi}\mathbf{W}_{r_{i+1}}(n)||^2 \\ &= (\mathbf{W}^H_{r_{i+1}}(n)\mathbf{W}_{r_{i+1}}(n))^{-1}\mathbf{W}^H_{r_{i+1}}(n)\mathbf{W}_{r_i}(n) \end{aligned} \tag{4.6}$$

After obtaining ϕ_0, in this way, the linear interpolation is applied between $\mathbf{W}_{r_i}(n)$ and $e^{j\phi_0}\mathbf{W}_{r_{i+1}}(n)$, instead of the original $\mathbf{W}_{r_{i+1}}(n)$. The corresponding equation is shown as

$$\mathbf{W}_l(n) = \frac{r_{i+1} - l}{m}\mathbf{W}_{r_i}(n) + \frac{l - r_i}{m}e^{j\phi_0}\mathbf{W}_{r_{i+1}}(n) \tag{4.7}$$

where $l \in \{r_i \dots r_{i+1}\}$ and $i \in \{0 \dots I-2\}$.

Within this framework, it is interesting to take another look at the above example in

Figure 4.5. The improved solution is now depicted in Figure 4.6, in which $\vec{OA'}$ represents the interpolated complex weight after the phase rotation. After phase compensation, $\vec{OA'}$ and the two complex weights of the selected tones have the same phase. As a result $|\vec{OA'}| = \frac{R_i+R_{i+1}}{2}$, and the performance degradation due to phase ambiguity is avoided.

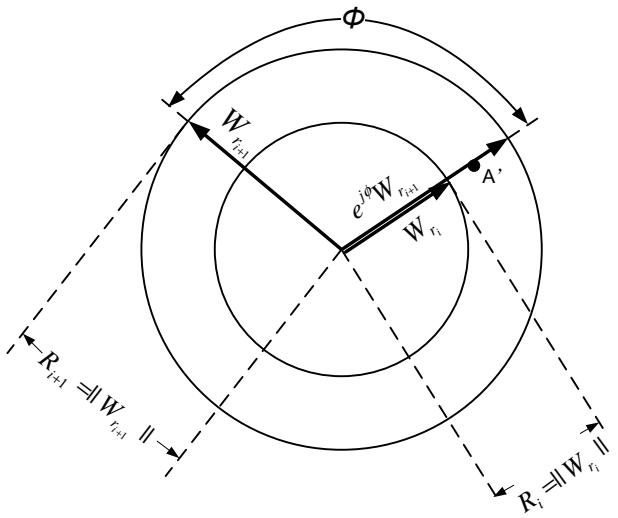

Fig. 4.6 Interpolation with phase-rotation.

Finally, we note that the weight vectors corresponding to the sub-carriers in the first group before r_0, and in the last group after r_{I-1} do not qualify for the application of the linear interpolation. This is because the term $\mathbf{W}_{r_{-1}}(n)$ or $\mathbf{W}_{r_I}(n)$, which would be needed as reference point to carry out the linear interpolation, are not defined. Therefore, for these "band-edge" group members, the flat-top interpolation is applied instead, by using $\mathbf{W}_{r_1}(n)$ and $\mathbf{W}_{r_{I-1}}(n)$.

4.1.4 Complexity Reduction

Several interpolation schemes were presented above for the purpose of reducing the implementation complexity of OFDM-based frequency domain beamforming using the RLS-CMA. In this section, the computational complexities corresponding to the original SIMO-OFDM beamforming system based on the RLS-CMA and the interpolated systems are evaluated and discussed.

The computational complexity of the RLS-CMA beamforming scheme, as presented in [13], is $3K^2 + 6K$ complex multiplies per iteration, where K indicates the number of

antennas in an array. The term $3K^2$ and $6K$ in this expression represent the complexity of the RLS-CMA weight adaptation and the beamforming, respectively. For the original system without complexity reduction, a distinct copy of the RLS-CMA must be run on each individual sub-carrier. Hence, the computational complexity of the system is written as follows:

$$\Gamma = N(3K^2 + 6K) = 3NK^2 + 6NK \tag{4.8}$$

where N is the number of the sub-carriers.

Since only the first weight vector in each group is updated by the RLS-CMA, the DFT-based interpolation, which is implemented via FFT and IFFT, reduces the system complexity as shown in the following equation:

$$\begin{aligned} \Gamma_{\text{DFT}} &= \frac{N}{M}(3K^2) + N(6K) + KN\log_2 N + KI\log_2 I \\ &\simeq \frac{3NK^2}{M} + 6NK + KN\log_2 N \end{aligned} \tag{4.9}$$

where M is the number of sub-carriers in each interpolation group, I is the number of groups and the terms $N\log_2 N$ and $I\log_2 I$ indicate the complexity of the N-point FFT and I-point IFFT, respectively. Since $I = \frac{N}{M}$, the latter term can be neglected. As presented in (4.9), the DFT-based interpolation is still very complex, due to the term $KN\log_2 N$, which for N large, exceeds the complexity value of the beamforming itself. From the perspective of complexity reduction, DFT-based interpolation scheme does not match the objective of this thesis. Therefore, the further analysis and discussion will only focus on the flat-top interpolation and the linear interpolation.

The complexity of the flat-top interpolation scheme is given by

$$\Gamma_{\text{Flat-Top}} = \frac{3NK^2}{M} + 6NK \tag{4.10}$$

Comparing this equation to (4.8), the complexity of the RLS-CMA term is reduced by a factor of M. However, this complexity reduction may decrease the system performance. Therefore, the size of the interpolation group, M, should be chosen wisely. Generally, beamforming on each subcarrier can be considered as a partial estimation of this sub-channel. Therefore, the characteristics of the channel affect the choice of M. For instance, if the channel is less frequency selective, a larger group size can be used, and vise versa.

As mentioned above, for the blind system, different choices of M should be tried, and the one achieving a desired level of performance with less complexity should be chosen.

For the linear interpolation scheme, the use of (4.7) adds a factor of $2NK$ to the complexity of the flat-top approach. We note that the evaluation of the phase factor in (4.6) only involves K multiplication and 1 division per group, for a total of $\sim\frac{NK}{M}$ operations in total. This factor is usually small in comparison to the factor $8KN$ and can be neglected. Therefore, the complexity of the linear interpolation scheme is approximately,

$$\Gamma_{\text{Linear}} = \frac{3NK^2}{M} + 8NK \tag{4.11}$$

4.2 Distributed Processing

Besides the use of frequency interpolation schemes, system complexity can also be reduced by considering processing across the space domain. As described in Chapter 2, the RLS-CMA can achieve a fast convergence rate at the cost of a high computational complexity, which is due to the recursive matrix inversion calculation. Specifically, if the antenna array contains K elements, the RLS-CMA requires on the order of K^2 operations per iteration. For K being large, the complexity rapidly becomes prohibitive. In this section, a distributed algorithm, which can reduce the system complexity with acceptable loss in system performance, is developed.

The distributed processing approach relies on the partitioning of the receiving array into sub-arrays and the use of a special approximation in the RLS-CMA. This allows a partial decoupling of the algorithm which can then be run on multiple processors with reduced overall complexity. Also since the RLS-CMA is run in parallel, and the weight vector for each sub-array has less elements, it is possible for the distributed process to achieve a faster convergence rate when compared to the original approach.

This distributed processing approach is also well-suited for collaborative beamforming in multi-node distributed relaying [18], which occurs in the framework of wireless *ad hoc* sensor networks. In these networks, a number of sensors randomly distributed in a local area, such as an office or a laboratory, collect useful information collaboratively with high energy efficiency. If sensor terminals are located sparsely enough and their number is large, the directivity of a "collaborative" beamformer can significantly exceed that of an individual terminal [18].

4.2.1 Algorithm Derivation

To develop a distributed processing scheme, we assume that the original K-element antenna array is partitioned into Q sub-arrays, each equipped with L antennas. In a distributed processing, the sub-arrays can be mounted on different cooperating relays as illustrated in Figure 4.7. In effect, if the relays exchange information and cooperate with each other, the beamforming ability of the whole system is enhanced compared to that of individual relays. The corresponding expression of the complete received signals from the K antennas at the n^{th} time iteration is given by

$$\mathbf{X}(n) = [\mathbf{X}_1^T(n) \dots \mathbf{X}_Q^T(n)]^T \tag{4.12}$$

where

$$\mathbf{X}_i^T(n) = [x_{i1}(n) \dots x_{iL}(n)] \tag{4.13}$$

is the received signal vector at the i^{th} sub-array. In a corresponding manner, the complete weight vector can be written as

$$\mathbf{W}(n) = [\mathbf{W}_1^T(n) \dots \mathbf{W}_Q^T(n)]^T \tag{4.14}$$

where

$$\mathbf{W}_i^T(n) = [w_{i1}(n) \dots w_{iL}(n)] \tag{4.15}$$

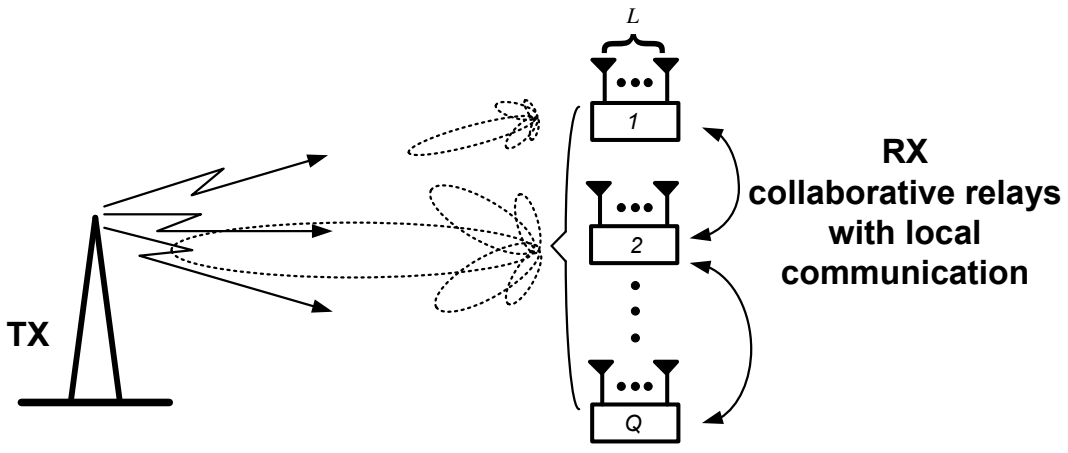

Fig. 4.7 Collaborative beamforming: Q sub-arrays, each equipped with L antennas.

In order to modify the RLS-CMA to accommodate distributed processing, we partition this algorithm into two sub-processes: a centralized process and a local process. That is, a centralized processor collects information from all the sub-arrays, performs certain"global" operations, and sends back the results to the sub-arrays for local processing. By utilizing the common information from the centralized processor, the local processor associated to each sub-array can run the RLS-CMA locally to obtain the optimal beamforming weight vector. Since the RLS-CMA is running locally, the dimensions of the computing matrices and vectors are relatively small, and consequently, the overall system complexity can be reduced. However, because of information sharing with the central processor, the beamforming performance of the complete K-antenna system is not dramatically affected.

The RLS-CMA was reviewed in Chapter 2, and the details of its derivation are described in [13]. As seen from (2.23) to (2.28), vector $\mathbf{Z}(n)$, which contains the received signal's information, is the only input vector to the RLS-CMA at a given iteration. Other quantities, such as $\mathbf{H}(n)$, $\mathbf{G}(n)$ and $\mathbf{P}(n)$, are internal parameters of the algorithm. Let $\mathbf{Z}_i(n)$ represent the input vector of the RLS-CMA for the i^{th}sub-array, where $i \in \{1 \dots Q\}$. As mentioned above, an information exchange should be done first with the central processor. The way to carry it out is to collect $\mathbf{X}(n)$ and $\mathbf{W}(n)$ as shown in (4.12) and (4.14), and apply (2.23) to obtain $\mathbf{Z}(n)$. We note that $\mathbf{Z}(n)$ can be partitioned as

$$\mathbf{Z}(n) = [\mathbf{Z}_1^T(n), \dots, \mathbf{Z}_Q^T(n)]^T \tag{4.16}$$

Besides information associated to the current i^{th} sub-array, $\mathbf{Z}_i(n)$ also contains information from the other sub-array. Indeed from the definition in (2.23), we find

$$\mathbf{Z}_i(n) = \mathbf{X}_i(n)\mathbf{X}^H(n)\mathbf{W}(n-1) \tag{4.17}$$

The term $\mathbf{X}^H(n)\mathbf{W}(n-1)$ contains common information from all the sub-arrays, and is included in each $\mathbf{Z}_i(n)$.

To simplify the information exchange between the central and local processors, we now take a closer look at the common information term in (4.17), which we denote as $Y^H(n)$:

$$
\begin{aligned}
Y^H(n) &= \mathbf{X}^H(n)\mathbf{W}(n-1) \\
&= [\mathbf{X}_1^H(n)\dots\mathbf{X}_Q^H(n)] \begin{bmatrix} \mathbf{W}_1(n-1) \\ \vdots \\ \mathbf{W}_Q(n-1) \end{bmatrix} \\
&= \sum_{i=1}^{Q} Y_i^H(n) \qquad (4.18)
\end{aligned}
$$

where

$$Y_i^H(n) = \mathbf{X}_i^H(n)\mathbf{W}_i(n-1) \qquad (4.19)$$

From the above equations, it is seen that the i^{th} sub-array only needs to transmit $Y_i^H(n)$ (4.19) to the centralized processor, which can then perform simple summation operation (4.18), to obtain the common information. Since $Y_i^H(n)$ is only a complex number, the data transmission process is much simplified.

Based on the above consideration, a distributed processing form of the RLS-CMA with Q sub-arrays can be developed as follows. After receiving its signal vector at the n^{th} time iteration, each sub-array computes its local beamforming output, i.e. $Y_i^H(n)$ in (4.19). Each sub-array then sends $Y_i^H(n)$ to the central processor, where the sum $Y^H(n)$ in (4.18) is obtained. Finally, the sum is sent back to each one of the sub-arrays, where it is used to perform the weight update, $\mathbf{W}_i(n-1) \rightarrow \mathbf{W}_i(n)$, based on a local realization of the RLS-CMA. This distributed algorithm is summarized in Table.4.1.

If we compare the above distributed realization of the RLS-CMA with the original form for $K = ML$ antenna array, we note important differences between them. Indeed, the distributed approach, the individual updating error term ξ_i of each sub-array takes the form

$$\xi_i(n) = 1 - \mathbf{W}_i^H(n-1)\mathbf{Z}_i(n). \qquad (4.20)$$

This is different from the error term in the complete original algorithm, as given by

$$
\begin{aligned}
\xi(n) &= 1 - \mathbf{W}^H(n-1)\mathbf{Z}(n) \\
&= 1 - \sum_{i=1}^{Q} \mathbf{W}_i^H(n-1)\mathbf{Z}_i(n). \qquad (4.21)
\end{aligned}
$$

Table 4.1 Summary of the distributed RLS-CMA

Initialize the algorithm by setting
$\mathbf{W}_i(0) = [1, 0_{1\times(K-1)}]^T$
$\mathbf{P}_i(0) = \delta^{-1} I_{L\times L}, \delta$ =small positive constant

For time iteration index $n = 1, 2, \ldots$
  For sub-array index $i = 1, 2, \ldots,$
    Local processing:
    $\mathbf{Y}_i^H(n) = \mathbf{X}_i^H(n)\mathbf{W}_i(n-1),$
    Centralized processing:
    $\mathbf{Y}^H(n) = \sum_{i=1}^{Q} \mathbf{Y}_i^H(n)$
    Local processing:
    $\mathbf{Z}_i(n) = \mathbf{X}_i(n)\mathbf{Y}^H(n),$
    $\mathbf{H}_i(n) = \mathbf{P}_i(n-1)\mathbf{Z}_i(n),$
    $\mathbf{G}_i(n) = \mathbf{H}_i(n)/(\lambda + \mathbf{Z}_i^H(n)\mathbf{H}_i(n)),$
    $\xi_i(n) = 1 - \mathbf{W}_i^H(n-1)\mathbf{Z}_i(n),$
    $\mathbf{W}_i(n) = \mathbf{W}_i(n-1) + \mathbf{G}_i(n)\xi_i^*(n),$
    $\mathbf{P}_i(n) = \lambda^{-1}\mathbf{P}_i(n-1) - \lambda^{-1}\mathbf{G}_i(n)\mathbf{Z}_i^H(n)\mathbf{P}_i(n-1).$
  end
end

Therefore, after each adaptive update, the parameters in these two forms of the RLS-CMA are modified differently. In practice, we find that the updating error of the local processor in (4.20) is larger than the updating error term in the complete RLS-CMA, which results in a loss of performance. This effect is further investigated in Chapter 5.

Finally, a block diagram of the proposed distributed form of the RLS-CMA is shown in Figure 4.8. In this distributed algorithm, the optimal weight vectors of the sub-arrays are iteratively obtained through the exchange of information between the local and centralized processors and the use of low-dimensional versions of the RLS-CMA running on the individual terminals.

4.2.2 Complexity Reduction

The complexity of this proposed distributed version of the RLS-CMA consists of two components. The first component results from the centralized information processing, and the other one results from the local processing. As shown in Table.4.1, the centralized processor collects the quantities $Y_i = \mathbf{X}_i^H(n)\mathbf{W}_i(n-1)$ from each one of the individual sub-array, i.e.

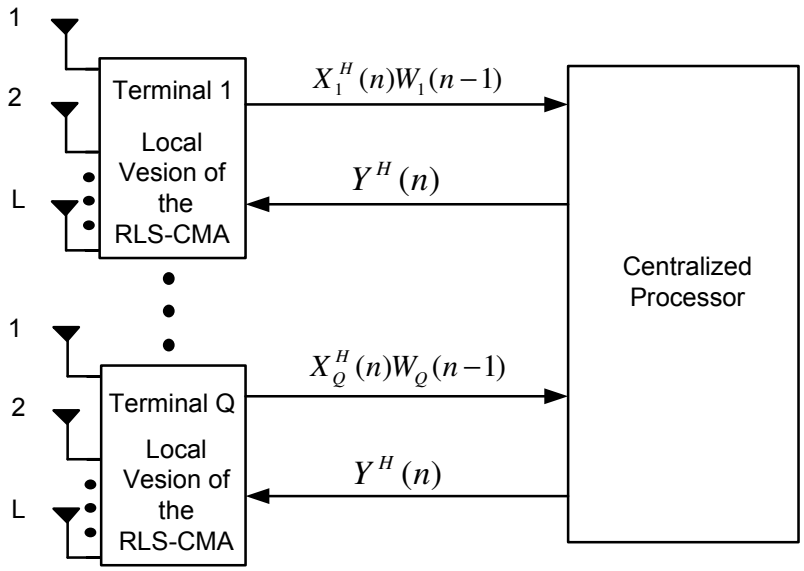

Fig. 4.8 Block diagram of distributed RLS-CMA.

for $i = 1, \ldots, Q$, and then sums them together to produce $Y(n)$ as shown in (4.18). This requires $QL = K$ complex multiplies per iteration, per each sub-carriers. The complexity of the local RLS-CMA processing is approximately $3QL^2 + 6QL$ complex multiplications per iteration for each OFDM sub-carrier, where L indicates the number of antennas in each sub-array. Therefore, the resulting complexity of the distributed process for a single carrier is approximately given by $3QL^2+7QL$. Finally, the computational complexity of the whole broadband blind beamforming system based on the distributed approach is obtained as

$$\Gamma_{\text{Distributed}} = NK(\frac{3K}{Q} + 7) \tag{4.22}$$

where N is the number of OFDM sub-carriers. Comparing (4.22) with (4.8), it is seen that the complexity of the RLS-CMA term is reduced by a factor of Q with the distributed approach.

If Q is chosen close to K, i.e., each sub-array terminal only contains a few antennas, we generally find that (see Chapter 5) even though the system complexity is much reduced, the performance of the system is poor. Therefore, the number of the antennas in each relay should be selected to achieve a compromise between the system complexity and the beamforming ability. If side information of the corresponding radio environment is available,

it may help in selecting the partition of the sub-array. For instance, when the channel is more frequency selective, we can choose a relatively larger group size to increase the group power, and vice versa.

Finally, we note that the sub-arrays need not have the same number of elements. The proposed distributed scheme can easily be modified to accommodate sub-arrays of different sizes. In this case, we can evaluate the complexity for each sub-array individually, and sum the results together.

4.3 Chapter Summary

In this chapter, complexity reduction techniques were developed for blind beamforming in SIMO-OFDM system based on the RLS-CMA. Flat-top interpolation and linear interpolation of the weight vectors in the frequency domain have been proposed. In the original system, a distinct copy of the RLS-CMA must be run on each individual sub-carriers. The application of frequency domain interpolation techniques, which allow the system to run the RLS-CMA only on some representative sub-carriers, decreases the system complexity. A distributed form of processing over the spatial domain was also presented. By partitioning the original array into several sub-arrays, and running the RLS-CMA locally, the size of the input signal correlation matrices of the sub-arrays is decreased, which is shown to result in a reduction of the system complexity. Hence, the system complexity is also reduced.

In the next chapter, a practical simulation example will be considered to evaluate these proposed schemes in terms of system complexity reduction.

Chapter 5

Simulation Results and Discussion

After presenting all the necessary technical concepts, such as adaptive beamforming algorithms and SIMO-OFDM techniques, simple schemes for reducing system complexity were developed in Chapter 4. In this chapter, we will validate the proposed complexity reduction schemes through numerical simulations. Specifically, these schemes will be applied to the up-link of a SIMO-OFDM blind beamforming system, operating over multi-path rayleigh fading channels. The particular focus of the simulation is on the SINR, and the bit error rate (BER). The main advantages and disadvantages of these proposed schemes will be discussed and summarized.

The present chapter is divided as follows, Section 5.1 introduces a number of parameters in the SIMO-OFDM beamforming model, and explains the characteristics of the statistical propagation channel model. Section 5.2, 5.3, and 5.4 provide numerical simulation results of the interpolation schemes, the distributed processing approach, and the combination of these two methods for complexity reduction, respectively.

5.1 Simulation Parameters and Channel Model

Before evaluating the performance of a complexity reduction scheme for the SIMO-OFDM blind beamforming application based on the RLS-CMA, we first need to define the main parameters of the system platform and the transmitted symbol mode. Also, the characteristics of the propagation channel need to be defined.

5.1.1 System Parameters

We assume that a 10-element uniform linear array (ULA) is employed at the RX side of the SIMO-OFDM system. The distance between adjacent elements in the array is set to half of the wavelength at the carrier frequency. The data are transmitted through uncoded OFDM symbols with $N = 64$ sub-carriers. The bandwidth of the transmitted signal is 1.2288MHz, with center frequency at 1GHz [30]. The length of the CP is 8 samples, which equals to 1/8 of the OFDM symbol duration, in order to eliminate ISI. Note that because an uncoded OFDM scheme is applied, each sub-carrier transmits independent data streams.

To mitigate co-channel interference (CCI) and noise, the original RLS-CMA and its proposed variations are used in the SIMO-OFDM system configuration (see Figure 3.5) to adapt the beamforming weights. Under otherwise indicated, the forgetting factor is set to $\lambda = 0.98$. Because a blind algorithm is used, the transmitted symbol should be defined to exhibit a special characteristic, namely the CM property. We use a quadrature phase shift keying (QPSK) signal constellation with a normalized energy, i.e. $E_S = E\{|S(k)|^2\} = 1$. The TX signals propagate through a multi-path SIMO channel (see below), and are received in the presence of additive white Gaussian noise and co-channel interference. The additive noise is modeled as complex circular Gaussian (i.e., independent Gaussian distributions for the real and imaginary parts) with zero mean and unit power, i.e. $E_N = \sigma_I^2 + \sigma_Q^2 = 1$. Under otherwise indicated, the $SNR = \frac{E_S}{E_N}$ is set to 10dB. The AOA of the interfering signal is set to $-10°$ and its power level is denoted as E_I.

5.1.2 Channel Model

Our system is tested under a dispersive propagation channel. The latter is generated by a statistical multi-path vector channel simulator [30], which evaluates the radio environment as multiple correlated Rayleigh fading channels. In the experiments reported below, all channels are assumed to have the same exponential power delay profile with $L = 3$ resolvable path. The corresponding AOAs of these dispersive signal paths are $-90°$, $90°$, $150°$ with angular spread $5°$, $10°$, $2°$, respectively. A sample realization of the channel is illustrated in Figure 5.1, which shows the magnitude response as a function of frequency for different antenna elements. We note that while the elements of the ULA are experiencing different fades, there is spatial correlation among them.

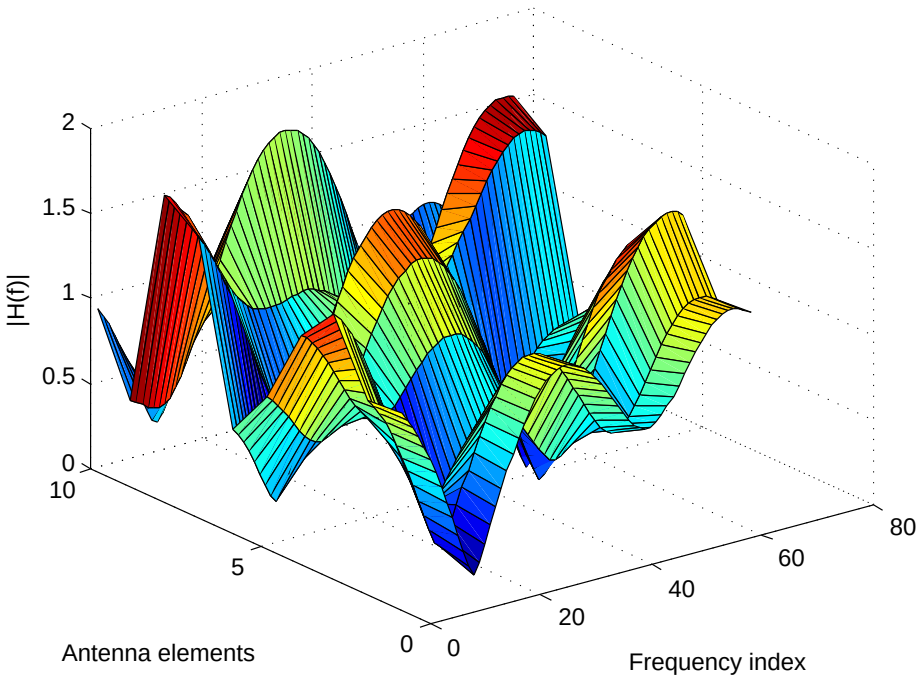

Fig. 5.1 Illustrative realization of the Rayleigh fading channel.

5.1.3 Performance Measure

The performance of the SIMO-OFDM systems with adaptive beamforming is evaluated in terms of the signal plus interference-to-noise ratio (SINR) and the bit error rate (BER) in uncoded transmission. For a given realization of the dispersive SIMO channel, the SINR for the n^{th} sub-carrier is given by

$$\mathrm{SINR}_n = \frac{E_S\,|\mathbf{W}_n^{\mathrm{H}}\mathbf{H}_{S,n}|^2}{\mathbf{W}_n^{\mathrm{H}}(\mathbf{H}_{I,n}P_I\mathbf{H}_{I,n}^{\mathrm{H}} + E_N\mathbf{I})\mathbf{W}_n}, \tag{5.1}$$

where $\mathbf{W}_n$ represents the beamforming weight vector used on the nth sub-carrier and $\mathbf{H}_{S,n}$ and $\mathbf{H}_{I,n}$ denote the $K \times 1$ vectors of complex channel coefficients for the desired source signal and the interference signal, respectively, corresponding to that frequency. We also define an overall broadband SINR by averaging SINR_n over all the sub-carriers, i.e. $\mathrm{SINR} = \frac{1}{N}\sum_{n=0}^{N-1}\mathrm{SINR}_n$. Referring to Figure 3.5, the BER is calculated by comparing the detected source data on the receiver side to the original transmitted source data.

5.2 Interpolation Methods

In this section, the proposed interpolation schemes across different sub-carriers are tested. As mentioned before, the middle tone sub-carrier is selected in each group, and different group sizes should be tried. Since the number of the OFDM tones in our system is set to 64, to make each group have the same bandwidth, the group size is selected as $M \in \{4, 8, 16\}$.

According to the analysis in Section 4.2, as M increases, more weight vectors are obtained by interpolation, and consequently the system complexity is reduced. The computational complexity of the direct and interpolated RLS-CMA schemes for different values of M, in unit of the number of complex multiplications per iteration, is shown in Table 5.1. The value given for $M = 1$ is obtained from (4.8) and corresponds to a direct application of the RLS-CMA to each sub-carrier (i.e. no interpolation). The values given for $M > 1$ are obtained from (4.10) for the flat top interpolation. The right-most column in the table shows the ratio $\Gamma_{\text{Interp}}(M)/\Gamma_{\text{Direct}}$, i.e., the reduction ratio of the original complexity. We note that the use of even a small value of $M = 4$ results in quite significant computational savings.

Table 5.1 Computational complexity of interpolated RLS-CMA.

M	Complexity	Complexity ratio
1	23040	1
4	8640	0.38
8	6240	0.27
16	5040	0.22

Figure 5.2 shows the time evolution of the SINR, averaged across all sub-carriers for the flat-top interpolation scheme. Since the RLS-CMA is applied, the system convergence rates are fast for all the different values of M. The main distinction among these plots is the SINR level after convergence, i.e., steady-state performance of the system. The steady-state SINR level for $M = 16$ is significantly lower than for the other three cases. This is because when the interpolation group size is too large, such as 16, it is possible that the group bandwidth becomes larger than the channel coherence bandwidth. Consequently, the weight vector obtained by interpolation may not be suitable for certain sub-carriers.

Note that, the steady-state SINR level for the 4 plots in Figure 5.2 are lower than the so called "optimal limit". The latter is obtained by averaging over the frequency the SINR resulting from the use of a special optimum weight vector, which is given for the n^{th}

sub-carrier by:

$$\mathbf{W}_{n,opt} = \frac{\mathbf{H}_{S,n}}{\mathbf{H}_{I,n} E_I \mathbf{H}_{I,n}^H + E_N \mathbf{I}} \tag{5.2}$$

This weight vector corresponds to the minimum-variance distortionless response (MVDR) beamforming algorithm [31], when the perfect channel knowledge of the desired signal and interference is available, and the noise power is known. The curve labeled "optimal" in Figure 5.2 is obtained by substituting the expression for $\mathbf{W}_{n,opt}$ in (5.2) into (5.1).

Results for the linear interpolation scheme, presented in Figure 5.3, show a similar performance as the flat-top interpolation for different group sizes. Hence, from these two figures, values of $M = 4$ and $M = 8$ yield satisfactory performance for this particular example.

It is interesting to look at the SINR performance from the frequency domain. Figure 5.4 and 5.5 show the steady-state SINR performance as a function of frequency for the flat-top and linear interpolation schemes, respectively. Both figures were obtained after stabilization of the adaptive weight vectors, i.e.,

$$\|\mathbf{W}(n) - \mathbf{W}(n-1)\|_\infty \leq 10^{-4} \tag{5.3}$$

where $\|\cdot\|_\infty$ denotes the infinity norm. Since the system under study is working over a frequency selective fading channel, the convergence level of the SINR corresponding to each tone varies greatly. Comparing the results from these two figures, the plots indicate that the system performance for the linear interpolation scheme is generally better than for the flat-top interpolation. This advantage is especially apparent when the group size is large, such as $M = 16$, and when the sub-carrier is experiencing deep fading. This is because the linear interpolation uses weight vectors at two representative frequencies to interpolate the weight vectors for sub-carriers between them, while the flat-top interpolation directly applies the selected tone's weight vector to other group members. For these reasons, the linear interpolation can generally achieve a better performance in a frequency selective fading environment. However, if the coherence bandwidth of the channel is very small, neither of these interpolation schemes can be applied to significantly reduce the system complexity.

Figure 5.6 and 5.7 show the uncoded average BER performance corresponding to the flat-top and linear interpolation schemes, respectively. Both these figures show that the

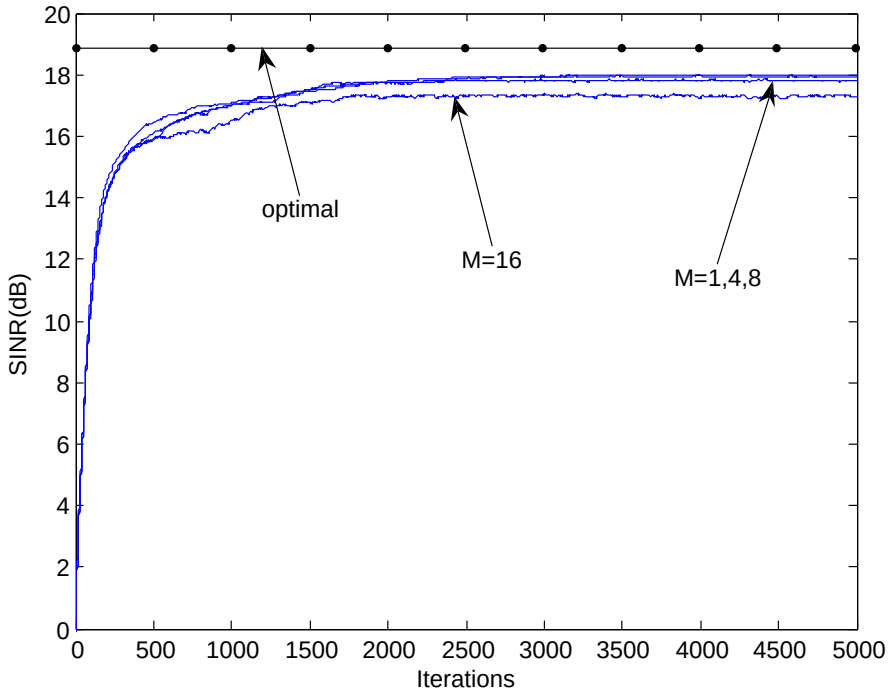

Fig. 5.2 Average SINR versus iteration number for flat-top interpolation.

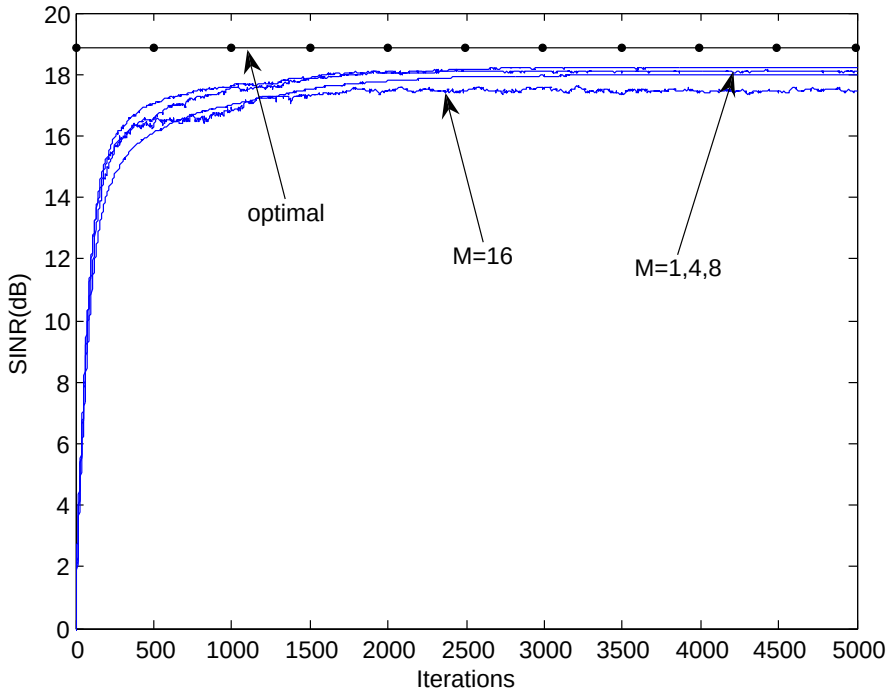

Fig. 5.3 Average SINR versus iteration number for linear interpolation.

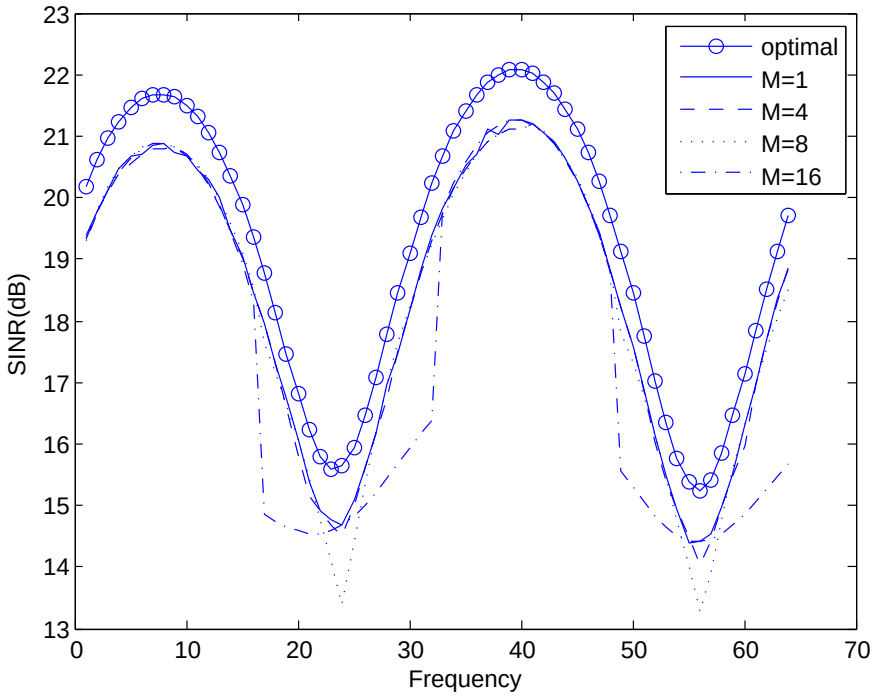

Fig. 5.4 Steady-state sub-carrier SINR versus frequency index for flat-top interpolation.

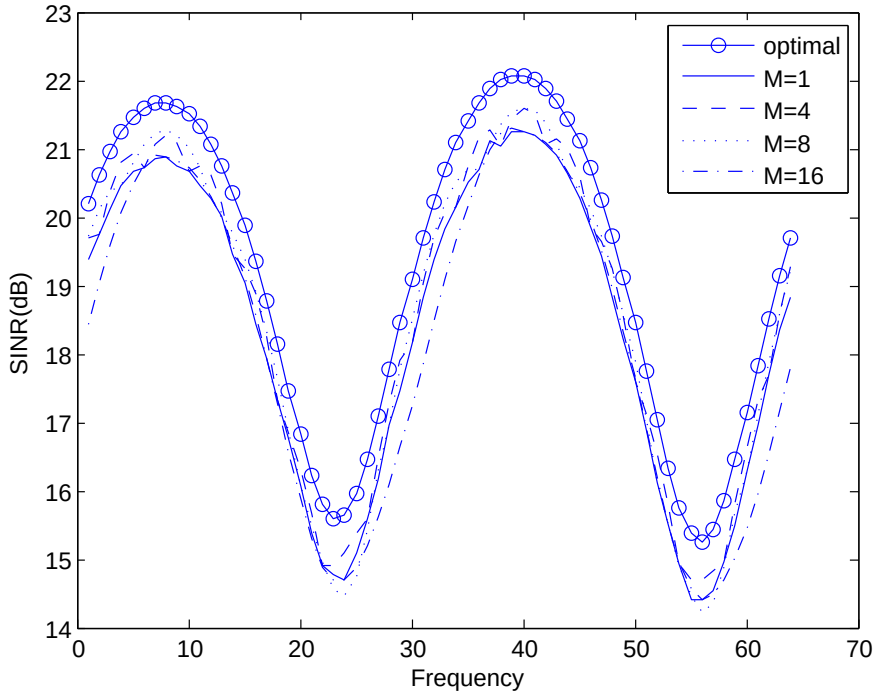

.

Fig. 5.5 Steady-state sub-carrier SINR versus frequency index for linear interpolation.

BER performance is decreasing with an increase in the sub-carrier group size, M. Compared to $M = 1$, use of $M = 8$ with flat-top interpolation leads to a 1dB performance loss at SNR= 5dB. For linear interpolation, this loss is only around 0.5dB.

An interesting situation is featured in Figure 5.7. Indeed, for the linear interpolation, when the group size is relatively small, in our case $M = 4$, it is possible that the weight vectors obtained by interpolation perform even better than those obtained by individual application of the RLS-CMA on each sub-carrier. It is because for some sub-carriers which are experiencing deep fading, the direct-adaptation of the weight vectors with the RLS-CMA may not properly converge, while the weight vectors obtained by interpolating adjacent sub-carriers, which do not experience deep fades, may form adequate beampatterns.

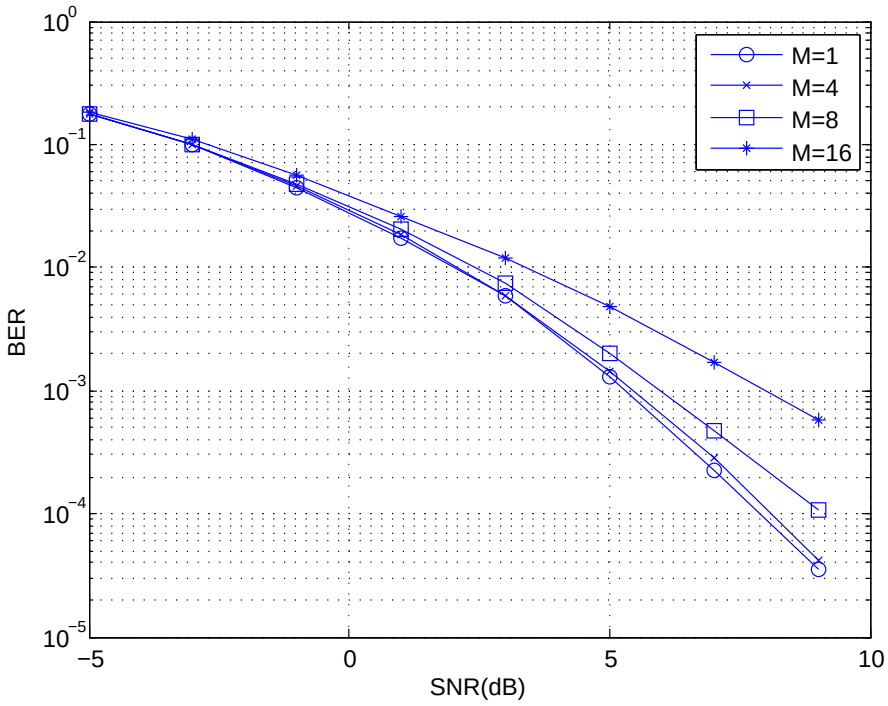

Fig. 5.6 BER of SIMO-OFDM beamforming based on RLS-CMA with flat-top interpolation.

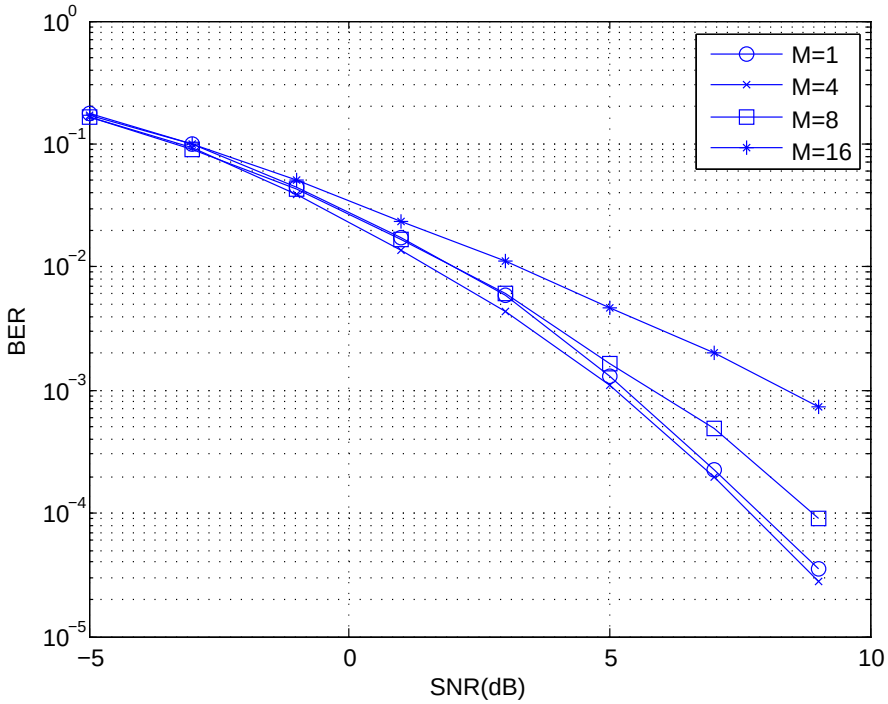

Fig. 5.7 BER of SIMO-OFDM beamforming based on RLS-CMA with linear interpolation.

5.3 Distributed Processing

The numerical simulation of the spatial domain distributed processing approach is made to verify the corresponding development in Section 4.3. As above, the original ULA is made up of 10 elements. For comparison purpose, two different partitions of this ULA are considered for distributed processing, namely (see Figure 5.8):

- Partition into two 5-element sub-arrays;
- Partition into 3 sub-arrays with 3, 3 and 4 elements, respectively.

According to the analysis in Section 4.3, the numerical values of the computational complexity for different sub-array partitions are shown in Table 5.2. As before, the complexity is measured in terms of the number of complex multiplications per iteration; the complexity ratio represents the reduction of complexity relative to original scheme (i.e., no partition). These figures show that the greater the number of sub-arrays we have, the greater the system complexity can be reduced.

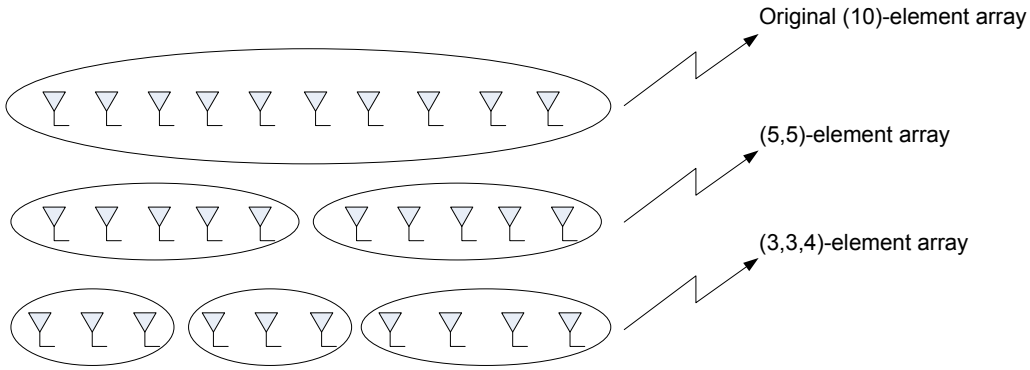

Fig. 5.8 Array partitions used for evaluation of the the distributed processing scheme.

Table 5.2 Computation complexity of distributed processing.

Array partition	Complexity	Complexity ratio
10	23040	1
$5-5$	13504	0.58
$3-3-4$	9344	0.40

As explained previously, the distributed processing approach cannot achieve the same level of performance as the original RLS-CMA based on the complete 10-element array. This is because each sub-array in the distributed processing scheme contains a weight vector with smaller dimension, and consequently, the residual error of the algorithm is larger. Correspondingly, as shown in Figure 5.9, without adjusting the forgetting factor λ of the RLS-CMA, the steady-state SINR of the original scheme is the highest among the three curves, but it has the slowest convergence rate. The (3,3,4) distributed scheme, on the other hand, has the lowest steady-state SINR, but the highest convergence rate. The resulting SINR from the two (5,5)-element array distribution is a compromise of the other two, which can achieve both reasonable steady-state and convergence rate.

By changing λ, the steady-states and the convergence rates of these curves can be adjusted in a constrained way. Since λ is the forgetting factor of the RLS-CMA, which controls the memory of the algorithm, the convergence rate is reduced corresponding to an increase in λ. For the purpose of comparing the three sub-array configurations, we tried different values of λ for each distribution. Figure 5.10 was generated to display the performance of the distributed RLS-CMA for the three different array configurations. In this figure, the horizontal axis represents the initial convergence slope, which indicates the

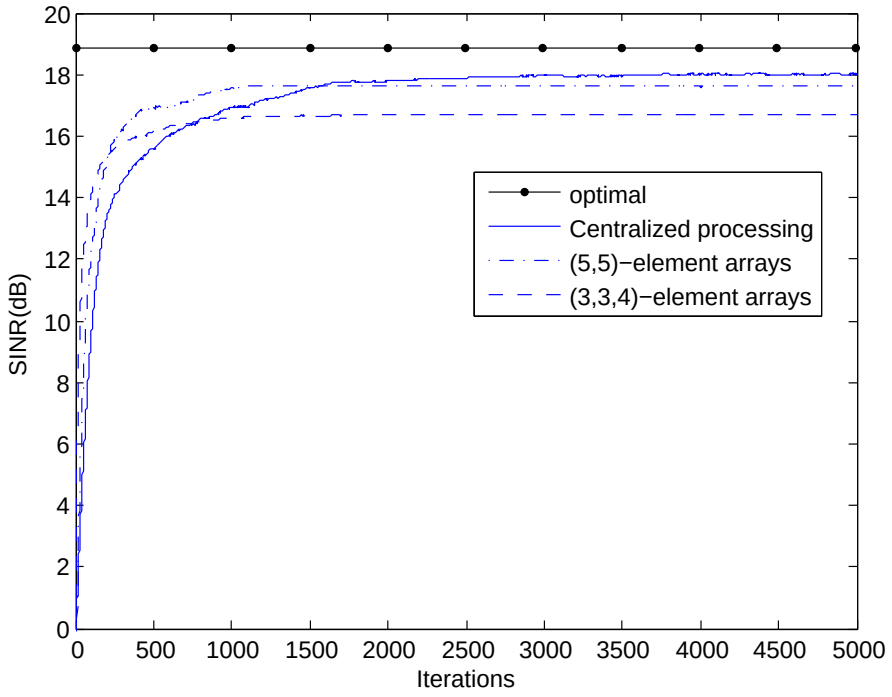

Fig. 5.9 Comparing average SINR for RLS-CMA based on different sub-array distributions (same $\lambda = 0.98$ for all configurations).

algorithm's convergence rate, and the vertical axis is the measurement of the corresponding steady-state SINR. The raw data with corresponding values of λ is presented in Appendix A. As shown in this figure, the (10)-element distribution can achieve the highest steady-state SINR, which cannot be obtained by using the other two distributions. For the comparison of the convergence rate, the (3,3,4) array distribution achieves the highest convergence rate in general, but at the cost of a significant reduction in steady-state SINR. As pointed out before, the (5,5) distribution achieves a compromise between these two extreme cases. When the value of λ is close to 1, such as 0.999, all three distributions need more time to converge. It is due to the increase of the algorithm's memory size. Indeed, because of the slow convergence rate, the steady-state of the maximum SINR cannot be obtained over the duration of the simulation experiment. Hence, in Figure 5.10, the SINR level goes down when λ is very close to 1. In practice, since the radio channel is changing rapidly and will "not wait for" the algorithm to achieve its steady-state beampattern, a value of λ very close to 1 could not be used in practice.

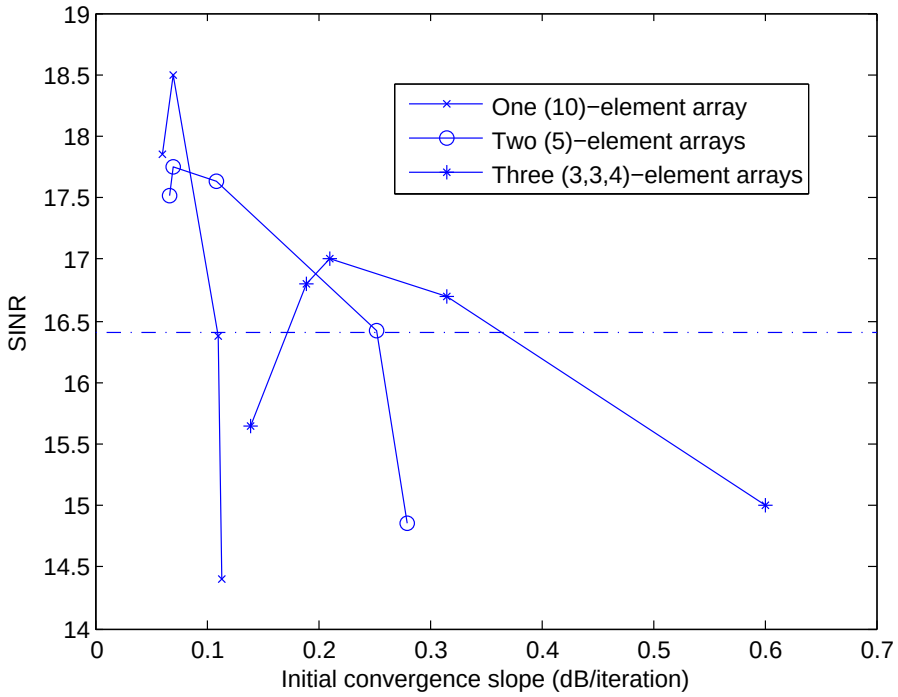

Fig. 5.10 Steady-state SINR of three different array distributions verses their corresponding initial convergence slope.

As shown in Figure 5.11, by adjusting the values of λ, the distributed processing and the centralized processing can achieve the same steady-state SINR (the dash-line in Figure 5.10), although the corresponding SINR level of 16.4dB is lower than the maximum of 18.5 with the 10-element configuration (see Figure 5.10). Both the distributed processing schemes, in this figure, have faster convergence rate than the centralized processing scheme. These facts are consistent with the corresponding statements we made for Figure 5.10.

Figure 5.12 shows the BER performance obtained with the steady-state beampattern corresponding to the results in Figure 5.9. The distributed algorithms show losses in the uncoded average BER performance as compared to the centralized processing scheme. For the same channel, the more groups we have, the larger degradation the BER performance suffers. This is because the distributed processing scheme, which contains less elements in each sub-array, is not as capable as the centralized processing scheme to form a directional beampattern.

In conclusion, we can summarize our observations as follows:

- The distributed processing scheme reduces the computational complexity and gener-

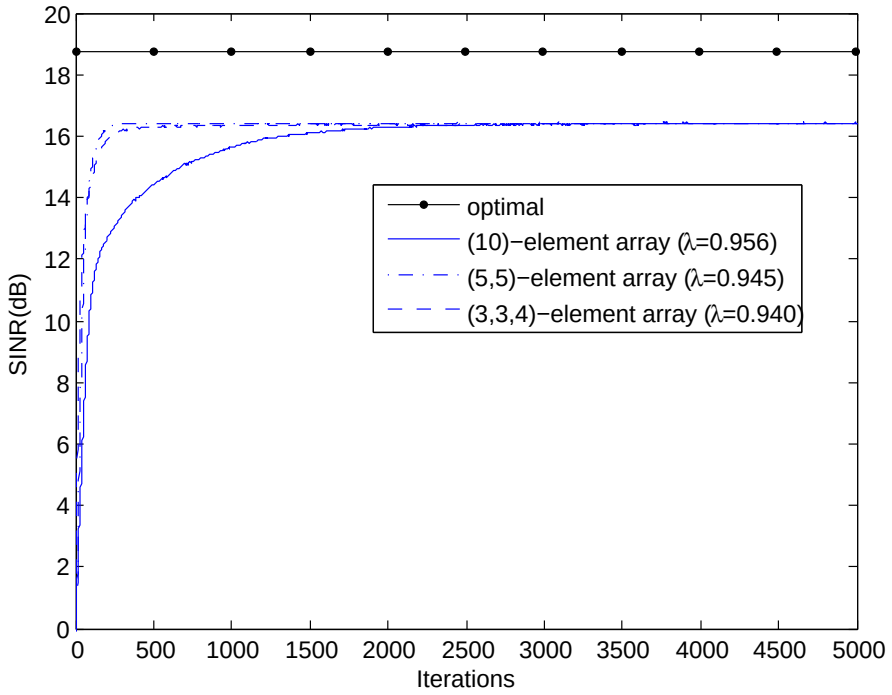

Fig. 5.11 Comparing average SINR on all sub-carriers for different sub-array distributions with different values of λ.

ally leads to a faster convergence rate, for a fixed forgetting factor, λ.

- There is a degradation in the maximum steady-state SINR and BER achievable with the distributed scheme, as compared to the original algorithm.
- By changing λ, the steady-state SINR and the convergence rate can be adjusted.

5.4 Combining Both Approaches

It is reasonable to assume that the combination of the interpolation approach with the distributed processing approach may provide additional flexibility in reaching a satisfactory trade-off between complexity and system performance. In this section, the performance of the combined scheme is evaluated. If the combined scheme can also achieve good BER performance and high steady-state SINR (i.e. consistent with the original system performance) it can be considered as a method for parallel simplification of the system computational complexity in both frequency and space domains.

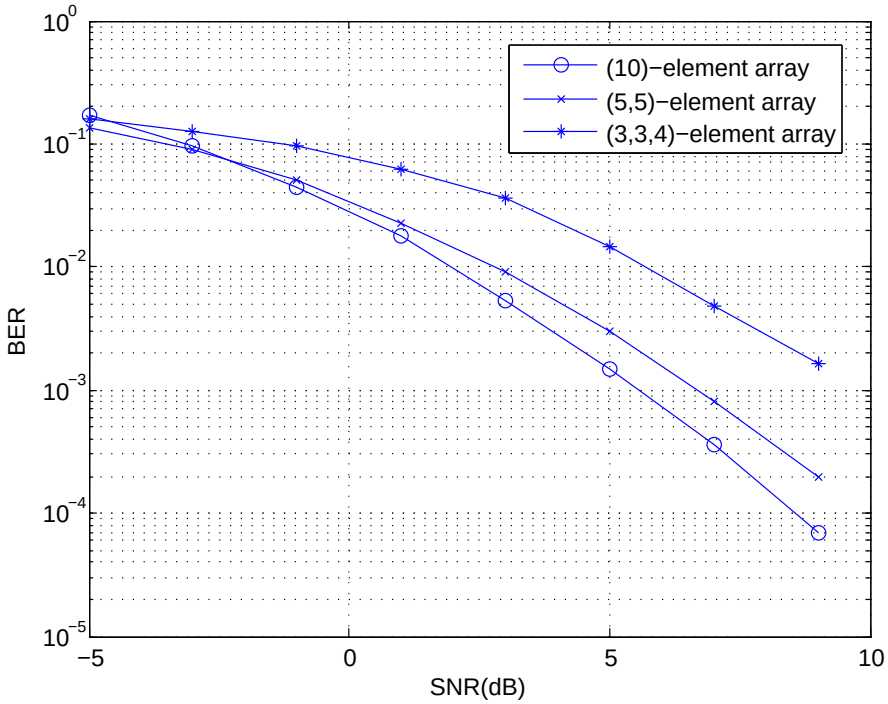

Fig. 5.12 Comparing BER performance of RLS-CMA based SIMO-OFDM beamforming for different sub-array distributions (same $\lambda = 0.98$ for all configurations).

As discussed above, the performance of both the interpolation and the distributed processing schemes are affected by the group sizes. For this combined processing, not all the sub-carrier group sizes and sub-array partitions are tested, only a typical example is considered. In the example, linear interpolation, which can achieve better system performance than flat-top interpolation, is applied with the sub-carrier group size equal to 4. The antenna array is partitioned into two 5-element sub-arrays. Corresponding to (4.8), (4.22) and Table 5.2, the complexity reduction of this combined scheme has a value of $\gamma = 0.25$ (i.e. 25% of the original system's complexity). The SINR and BER performance of the combined scheme and the original system are shown in Figure 5.13 and 5.14, respectively. As shown in Figure 5.13, the combined application of both complexity reduction schemes results in higher convergence rate, but smaller steady-state SINR. In Figure 5.14, we see that the degradation of the BER with the combined scheme is of the order of 1dB, as compared to the original algorithm. This result is consistent with the above discussion of the individual complexity reduction methods.

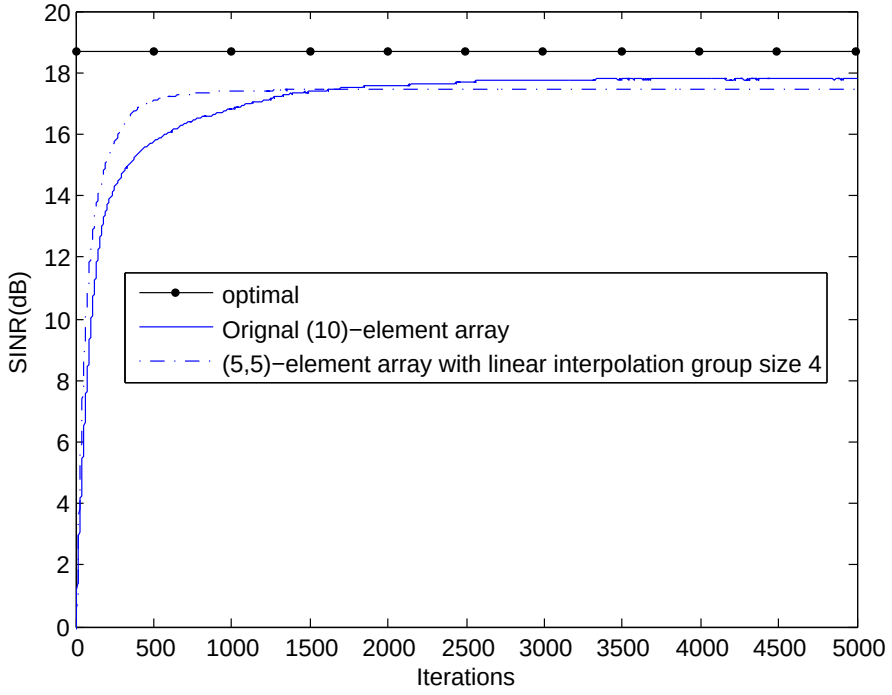

Fig. 5.13 Comparing average SINR on all sub-carriers of combined scheme with the original algorithm ($\lambda = 0.98$).

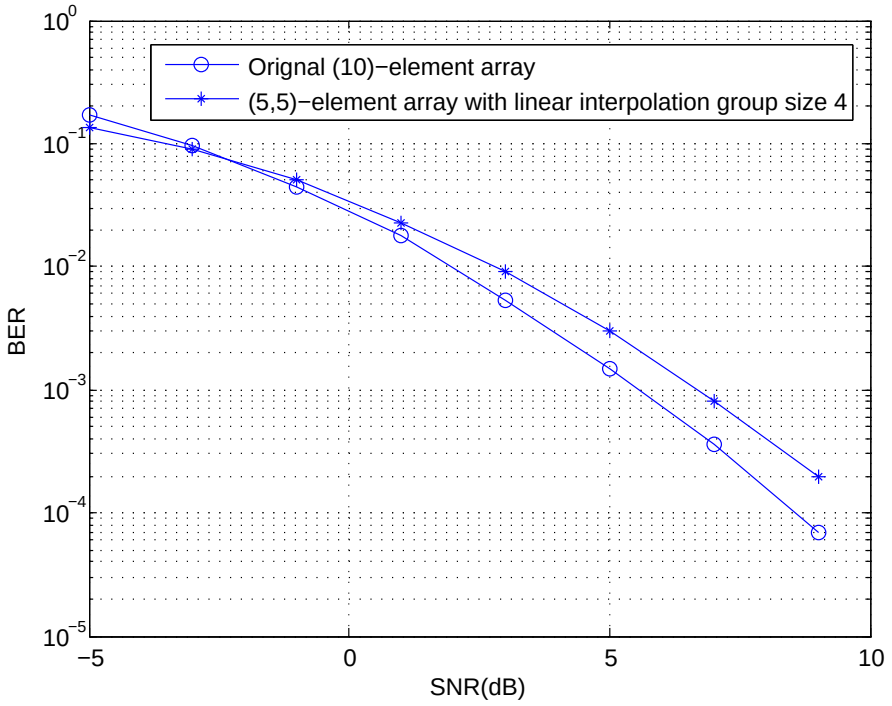

Fig. 5.14 Comparing BER of RLS-CMA based SIMO-OFDM beamforming of combined scheme with the original algorithm ($\lambda = 0.98$).

5.5 Chapter Summary

In this chapter, numerical simulation experiments have been used to evaluate the steady-state SINR, the SINR convergence rate and the BER performance of the proposed complexity reduction schemes. By selecting different interpolation group sizes and sub-array configurations, the performance of both the frequency interpolation and the distributed processing schemes were evaluated and compared with that of the original system. We can summarize our results by noting that both these frequency domain and space domain schemes can indeed reduce the system complexity. The cost incurred is a loss in the achievable system performance. By properly selecting the interpolation parameters or the partitioning configuration, the system performance is not degraded below tolerable levels. Also, for distributed processing, due to the smaller dimension of the weight vectors, the convergence rate of the algorithm is increased. In addition, we have verified that by combining these two schemes, the system complexity can be further reduced with small losses in BER performance.

Chapter 6

Conclusion and Future Work

The main objective of this research was to investigate solutions in both the frequency domain (sub-array interpolation) and the spacial domain (antenna array distribution) to reduce the processing complexity of SIMO-OFDM beamforming system for wireless communication, based on the blind RLS-CMA algorithm and operating in a slowly fading radio channel.

6.1 Thesis Overview

- In Chapter 2, adaptive beamforming techniques were reviewed, and classified into two categories, i.e. non-blind algorithms and blind algorithms. Since the non-blind algorithms suffer from consuming precious channel bandwidth, and the LMS based CMA in the blind category has slow convergence rate, the RLS-CMA was adopted for our system.

- In Chapter 3, the basic OFDM technique was briefly reviewed. A SIMO-OFDM beamforming system was then developed, which can achieve good performance over a slowly fading frequency selective channel. However, the system operation complexity was relatively high, and this motivated our work in the remaining chapters, i.e. reducing the complexity of this proposed system while maintaining an acceptable level of performance.

- In Chapter 4, to achieve this goal, the frequency domain flat-top interpolation, linear interpolation and the space domain distributed processing schemes were proposed

and developed in detail.

- In Chapter 5, simulation results of a practical example were presented and discussed. Different values of the main system parameters were tried to find the best trade-off between complexity reduction and system performance. These include: choice of representative sub-carrier in the interpolation group, the interpolation group size and different partitions of the distributed algorithm. The combined utilization of the interpolation and distributed processing scheme was also tested.

6.2 Main Contributions

To achieve the objectives, the following novel algorithms were proposed and evaluated by means of Monte Carlo simulations.

- Interpolation techniques that exploit the coherence bandwidth of the radio channel: in these schemes only the weight vectors at representative frequencies are adapted while interpolation is used to obtain the intermediate weight vectors. Two interpolation schemes were considered, namely: (i) flat-top interpolation and (ii) linear interpolation.

- Distributed processing approach: This approach relies on the partitioning of the receiving array into sub-arrays and the use of a special approximation in the RLS-CMA. The latter allows a partial decoupling of the algorithm which can then be run on multiple processors with reduced overall complexity.

As explained and verified in the thesis, if the proper interpolation group size and the representative tones are selected in the frequency domain or a proper partition of the sub-arrays is chosen in the space domain, both of these methods can reduce the computational complexity of the system without too much effect on the system performance. The simulation results enable us to conclude that both of these complexity reduction schemes can be utilized as good solutions to reduce the system complexity in practical application of SIMO-OFDM systems.

6.3 Future Research Direction

Further work is needed to develop practical guidelines for the selection of relevant system parameters, i.e. group size and sub-array configuration in application over true radio channels. The final solution might involve a learning period, during which relevant characteristics of the channel (e.g. coherence bandwidth) are gathered and used to make the appropriate choice of parameters, so as to reduce the computational complexity of the system without exceeding an acceptable performance degradation. For time-varying channels, further analysis would be needed to better understand the fundamental decoupling approximation used in Section 4.2 to derive the decentralized processing scheme. Presently, the validity of this approximation is only supported by a limited set of experimental results. It would be interesting to quantify the performance loss resulting from this approximation and to characterize its domain of validity, i.e. what condition must be satisfied for the resulting algorithm to behave like the original RLS-CMA.

To improve the performance of the proposed techniques for blind SIMO-OFDM beamforming, some extra work could be done in the future. First, channel coding and interleaving schemes should be added to mitigate the effects of error bursts, which are due to the deep fading of the frequency selective channel. As mentioned in Chapter 3, this goal can be pursued through the application of convolutional and Reed-Solomon codes to the system.

Practical OFDM systems are often semi-blind, i.e. partial knowledge of the propagation channel can be obtained at the RX side. Therefore, this information may help recognize some characteristics of the radio channel, and consequently guide the selection of representative sub-carriers, proper group sizes or partitions of the distributed processing to improve the system performance.

In a practical application of SIMO-OFDM, the synchronization impairments, which was omitted in the thesis for simplification, should be considered. Since these impairments compromise the orthogonality of the channel, ICI between the sub-carriers may appear, and consequently, some corresponding techniques should also be applied to achieve the frequency synchronization.

References

[1] A. Goldsmith, *Wireless Communications*, NY: Cambridge University Press, 2005.

[2] A. Paulraj, R. Nabar, and D. Gore, *Introduction to Space-Time Wireless Communications*, NY: Cambridge University Press, 2003.

[3] R. V. Nee and R. Prasad, *OFDM for Wireless Multimedia Communications*. Boston: Artech House, 2000.

[4] Y. Li, and G. Stuber, *Orthogonal Frequency Division Multiplexing for Wireless Communications*, Springer Science, 2006.

[5] A. Peled and A. Ruiz, "Frequency domain data transmission using reduced computational complexity algorithms," *IEEE Int. Conf. on Acoustics, Speech, and Signal Processing (ICASSP)*, Denver, USA, pp. 964-967, Apr. 1980.

[6] F. W. Vook and K. L. Baum, "Adaptive antennas for OFDM," *IEEE 48th Vehicular Technology Conf.*, vol. 1. pp. 606-610, May 1998.

[7] V. Venkataraman, R. E. Cagley and J. J. Shynk, "Adaptive beamforming for interference rejection in an OFDM system," *The 37th Asilomar Conf. on Signal, System and Computers*, vol. 1, pp. 507-511, Nov 2003.

[8] H. Liu, and Q. Feng, "A blind adaptive beamforming for OFDM system," *Canadian Conf. on Electrical and Computer Engineering (CCECE)*, pp. 1208 - 1211, May 2005.

[9] S. Haykin, *Adaptive Filter Theory*, 4th ed. NJ: Pentice-Hall, 2002.

[10] R. P. Gooch and J. D. Lundell, "The CM array: an adaptive beamformer for constant modulus signals" in *Proc. IEEE Int. Conf. Acoust., Speech, Signal Processing*, pp. 2523-2526, Apr. 1986.

[11] T. E. Biedka, W. H. Tranter, and J. H. Reed, "Convergence analysis of the least squares constant modulus algorithm in interference cancellation applications" in *IEEE Trans. Signal Processing*, vol. 48. pp. 491-501, March 2000.

[12] Y. X. Chen, Z. Y. He, T. S. Ng, and P. C. K. Kwok, "RLS adaptive blind beamforming algorithm for cyclostationary signals", *Electron. Lett.*, Vol. 35, pp. 1136-1138, July 1999.

[13] Y. X. Chen, T. Le-Ngoc, B. Champagne, and C. Xu, "Recursive least squares constant modulus algorithm for blind adaptive array", *IEEE Trans. Signal Processing*, Vol. 52, pp. 1452-1456, May 2004.

[14] C. A. R. Fernandes, G. Favier, and J. C. M. Mota, "Decision directed adaptive blind equalization based on the constant modulus algorithm," *Signal, Image and Video Processing* , vol. 1, pp. 333-346, Oct. 2007.

[15] "802.11, Part 11: Wireless LAN Medium Access Control (MAC) and Physical Layer (PHY) specifications: High-speed Physical Layer in the 5 GHz Band", IEEE standard, Sept. 1999.

[16] T. Haustein, S. Schiffermuller, V. Jungnickel, M. Schellmann, T. Michel and G. Wunder, "Interpolation and noise reduction in MIMO-OFDM a complexity driven perspective", *IEEE Trans. on Signal Processing*, vol. 1, pp. 143-146, Aug. 2005.

[17] M. Borgmann and H. Bolcskei "Interpolation-based efficient matrix inversion for MIMO-OFDM receivers", in *Proc. 38th Asilomar Conf. Signals, Systems, Computers,* Pacific Grove, CA, (invited paper), vol. 2, pp. 1941- 1947, Nov. 2004.

[18] H. Ochiai, P. Mitran, H. V. Poor, and V. Tarokh, "Collaborative beamforming for distributed wireless ad hoc sensor networks," *IEEE Trans. Signal Processing*, vol. 53, pp. 4110-4124, Nov. 2005.

[19] P. R. P. Hoole, D. Phil. Oxon, *Smart Antennas and Signal Processing for Communications, Biomedical and Radar Systems*, WIT Press, 2001.

[20] A. Mathur, A. V. Keerthi, and J. J. Shynk, "A variable step-size CM array algorithm for fast fading channels", *IEEE Trans. Signal Processing*, vol. 45, pp. 1083-1087, Apr. 1997.

[21] J. R. Barry, and A. Batra, "A multidimensional phase-locked loop for blind equalization of multi-input multi-output channels," *Int. Conf. on Communications,* Dallas, USA, vol. 3, pp. 1307-1312, June 1996.

[22] K. N. Oh, and Y. O. Chin, "Modified constant modulus algorithm: blind equalization and carrier phase recovery algorithm," *Int. Conf. on Communications,* Seattle, USA, vol. 1, pp. 498-502, June 1995.

[23] J. Yang, J. J. Wrner, and A. Dumont, "The multimodulus blind equalization and its generalized algorithms" *IEEE J. on Selected Areas in Communcations,* vol. 20, pp. 997-1015, June 2002.

[24] J. T. Yuan and K. D. Tsai, "Analysis of the multimodulus blind equalization algorithm in QAM communication systems", *Int. Symp. on Communications and Information Technologies*, Sappom, Japan, pp. 1427-1431, Oct. 2004.

[25] Y. Li and N. R. Sollenberger, "Adaptive antenna arrays for OFDM systems with cochannel interference", *IEEE Trans. on Communications,* vol. 47, pp. 217-229, Feb. 1999.

[26] Y. F. Chen, "Adaptive antenna arrays for the co-channel interference cancellation in OFDM communication systems with virtual carriers", *Proc. IEEE Sensor Array Multichannel Signal Process,* pp. 393-397, Aug. 2002.

[27] K. Wong, R. S. Cheng and K. B. Letaief, "Adaptive antennas at the mobile and base stations in an OFDM/TDMA system", *IEEE Trans. on Communications,* vol. 49, pp. 195-206, Jan. 2001.

[28] J. G. Proakis, *Digital Communications,* 4^{th} *ed.* McGraw-Hill, 2001.

[29] A. V. Oppenheim, A. S. Willsky, and S. H. Nawab, *Signals and Systems,* 2^{nd} *ed.* Prentic-Hall, 1983.

[30] A. Stephenne and B. Champagne, "Effective multi-path vector channel simulator for antenna array systems" *IEEE Trans. on Vehicular Technology*, vol. 49, Nov. 2000.

[31] H. L. Van Trees, *Optimum Array Processing*, John Wiley & Sons, 2002.

Appendix A

Raw data for Figure 5.10

Table A.1 (10)-element array

λ	Initial slope	Steady-state SINR
0.995	0.060	17.85
0.990	0.070	18.50
0.955	0.109	16.38
0.920	0.115	14.40

Table A.2 (5,5)-element array

λ	Initial slope	Steady-state SINR
0.995	0.066	17.51
0.990	0.070	17.75
0.980	0.110	17.63
0.945	0.252	16.42
0.820	0.280	14.85

Table A.3 (3,3,4)-element array

λ	Initial slope	Steady-state SINR
0.995	0.140	15.65
0.992	0.190	16.80
0.990	0.210	17.00
0.962	0.315	16.70
0.820	0.600	15.00